DESIGN OF A WIDEBAND AND BI – DIRECTIONAL TRANSDUCER FOR UNDERWATER COMMUNICATIONS

A THESIS
SUBMITTED TO THE DEPARTMENT OF ELECTRICAL AND ELECTRONICS ENGINEERING
AND THE INSTITUTE OF ENGINEERING AND SCIENCES
OF BILKENT UNIVERSITY
IN PARTIAL FULLFILMENT OF THE REQUIREMENTS
FOR THE DEGREE OF
MASTER OF SCIENCE

By
Işıl Ceren Elmaslı
April 2007

I certify that I have read this thesis and that in my opinion it is fully adequate, in scope and in quality, as a thesis for the degree of Master of Science.

Prof. Dr. Hayrettin Köymen (Supervisor)

I certify that I have read this thesis and that in my opinion it is fully adequate, in scope and in quality, as a thesis for the degree of Master of Science.

Prof. Dr. Ayhan Altıntaş

I certify that I have read this thesis and that in my opinion it is fully adequate, in scope and in quality, as a thesis for the degree of Master of Science.

Dr. Satılmış Topçu

Approved for the Institute of Engineering and Sciences:

Prof. Dr. Mehmet B. Baray
Director of Institute of Engineering and Sciences

ABSTRACT

DESIGN OF A WIDEBAND AND BI – DIRECTIONAL TRANSDUCER FOR UNDERWATER COMMUNICATIONS

Işıl Ceren Elmaslı
M.S. in Electrical and Electronics Engineering
Supervisor: Prof. Dr. Hayrettin Köymen

April 2007

A two ceramic layer stacked transducer structure for short range underwater communications at high frequencies is studied in this work. The structure has a wide bandwidth of one octave and operates at 350 kHz center frequency. Transducer structure inherently has two electrical and two acoustic ports. Ceramic layers are matched to water load through quarter wavelength thick matching layers on each radiating face. Using electrical ports separately to compensate for the large acoustic length of the structure in water is also investigated. It is shown that the wide bandwidth operation can be maintained. The beamwidth of the structure is narrow due to end - fire effect of two back – to – back radiating elements.

Keywords: Acoustic underwater communication, transducer, wideband, wide beamwidth, infinite rigid baffle, composite piezoelectric.

ÖZET

SUALTI İLETİŞİMİ İÇİN GENİŞ BANDLI VE ÇİFT – YÖNLÜ AKUSTİK ÇEVİRİCİ MODELLEMESİ

Işıl Ceren Elmaslı
Elektrik ve Elektronik Mühendisliği Bölümü Yüksek Lisans
Tez Yöneticisi: Prof. Dr. Hayrettin Köymen

Nisan 2007

Bu tezde yüksek frekanslı kısa mesafe sualtı iletişimi için iki seramik katmanlı çevirici yapısı irdelendi. Yapının bir oktav genişliğinde çalışma bandı bulunmaktadır ve merkez çalışma frekansı 350 kHz'dir. Çevirici yapısında iki elektriksel, iki akustik port vardır. Seramik katmanlar her bir ışıma yapan yüzeyden su yüküne çeyrek dalga kalınlığındaki eşleştirici katmanlar aracılığıyla eşlenmişlerdir. Yapının sudaki uzun akustik boyunu dengelemek için elektriksel portların birer birer kullanılması incelenmiştir. Bu şekilde geniş bir bant aralığında çalışma sağlanmıştır. Yapının hüzme genişliği arka arkaya ışıyan elemanlardan dolayı dardır.

Anahtar Kelimeler: Akustik sualtı haberleşmesi, çevirici, geniş bant, geniş hüzme genişliği, sonsuz sert sınır, karma piezoelektrik.

Acknowledgements

I would like to express my gratitude to my supervisor Prof. Dr. Hayrettin Köymen for his instructive comments in the supervision of the thesis.

I would like to express my special thanks and gratitude to the jury members Prof. Dr. Ayhan Altıntaş and Dr. Satılmış Topçu for evaluating my thesis.

I would also like to express my thanks to my parents and my husband Alper for their endless love and support throughout my life.

Contents

List of Figures

List of Tables

Chapter 1

Introduction

Underwater acoustic (UWA) communications is an interesting research field that shapes the abilities of people in shallow and deep waters. Preserving communication for long duration with a light weight and low battery power consumption becomes increasingly important for scuba divers, petrol inspectors and pollution analyzers [1]. Furthermore, the developments in piezoelectric materials make it possible to have more effective underwater communication applications.

1.1 Historical References

Leonardo Da Vinci is quoted to be the first one, who though it was possible to send and receive information in underwater. His discovery concerns the possibility of detecting a distant ship with a long tube submerged under the sea [2]. UWA communication systems are being used in underwater since 1905 [3]. A wire link between the diver and a surface communication point was used for voice communication [4]**.** Following the German submarine menace of 1st World War, researches are focused on the behavior of sound in underwater; besides its effects on submarine, surface ship, weaponry, and target locations [5]. SOund NAvigation

and Ranging term, “SONAR” was first used at that time. Echosounders are developed to detail bathymetry. Seismic and sidescan - sonar systems are evolved to map the sea floor and subsurface [6].

The U.S. Navy developed an underwater telephone to communicate with submarines by 1945 [2]. It was using a single - sideband suppressed carrier amplitude modulation in the range of 8 – 11 kHz. It was sending acoustic signals to several kilometers.

There has been a growing interest in the UWA communications in various application areas such as telemetry, remote control, and speech or image transmission in recent years. The bandwidth efficiency of proposed systems becomes an important issue in UWA communications [6].

1.2 Communication Channel

Acoustic propagation has physical constraints on the AUW channel, such as: Limited, range – dependent bandwidth, time varying multipath and low speed of sound (1500 m/sec) [7], [8]. The propagation range is low for high frequency channels. As a result, it is possible to send large bandwidth data over short distances.

On the other hand, the AUW systems includes barriers such as battery power, half – duplex communication and transducer bandwidth. The effective bandwidth of a transducer depends on the characteristics of materials used.

1.3 Piezocomposite Materials

The piezoelectric effect was discovered by Jacques and Pierre Curie in 1880. They found that when certain crystals are subjected to mechanical strain, they become electrically polarized and the degree of polarization is proportional to the applied strain [9]. The piezoelectric materials can convert mechanical energy into electrical and vice versa.

Piezoelectric ceramics are used in AUW transducer designs. The easy fabrication, lightweight and thickness properties, and thus high – sensitivity with better pressure stability characteristics are better than other transduction materials properties [10].

We prefer piezocomposite materials rather that piezoelectric ceramics because they offer increased sensitivity, broader bandwidth, improved impedance match to water and higher efficiency [11], [12]. Composite piezoelectric materials can be prepared by combining a piezoelectric ceramic with polymer layers [12], [13]. The geometry of these materials provides advantages such as high electromechanical coupling constant and acoustic impedance that can be matched to water through a matching layer. For the thesis, we prefer 30% PZT-5A and 70% stycast for the 1 – 3 composite ceramic layers.

1.4 Designing Transducer

Studies of Rayleigh, Pochammer, Chree, Lové, Bancroft and Davies developed the area of sound speed variability in rods [14]. The techniques based on implementation of piezoelectric transducer materials to transmission lines including transformer is introduced by Mason – the Mason Model, Redwood – the Redwood Model and Krimholtz, Leedom and Matthaei – the KLM Model [15].

Previous developments of transducer designs for underwater applications have shown that matching the structure to water with multiple matching layers is necessary for achieving a wide bandwidth, such as in the case of *thin disk*. The thin disk design highly depends on the properties of ceramic layers [16]. A common thin disk design is made by fixing two quarter – wavelength matching layers and connecting the structure to a half – wavelength PZT material. The thin disc structure is air – backed. It is immersed into water directed from a vibrating face. The thin disk design introduces narrow beamwidth reception characteristics which is advantageous in overcoming situations where multipath is a problem. The model is proper for using in upper band of 100 kHz to 1 MHz frequency region [17].

Another well – known transducer model is *piston type*. It is used for low frequency applications, 0 – 30 kHz. The model is constructed with metal – end pieces that act as resonators with central section of ceramic layer acting as the motor. Fabrication of the model is investigated by Neppiras [18] and Stansfield [19]. A broadband transducer is achieved by adding a quarter – wavelength matching layer to the loaded side of the structure. It has been shown that careful addition of other matching layers modifies the behavioral aspect of the transducer.

Many developers followed the former ones in developing piston – structure acoustic transducers. However, the problem with piston structures, mainly for low – frequency applications remained constant: Their voluminous and high weight due to structure being air backed limited the effective propagation areas and conditions of their application areas.

1.5 A Wideband and Bi – directional Transducer Design for Underwater Communications

This work concerns design of a short range, wideband transducer. The band of the transducer is relatively wide when compared to other transduction elements.

Designing an omni – directional wideband transducer is not achievable for most of the transducer structures. The beamwidth of the transducer structure depends on the value of the radius to thickness ratio which is high compared to the wavelength of water. It also depends on the operational frequency.

The proposed transducer is achieved by connecting two quarter – wavelength composite piezoelectric layers with a thin aluminium layer. The piezocomposite layers are matched to water with quarter wavelength matching layers on both sides; besides they introduce two electrical ports to the transducer structure. We constructively add the electrical signals sensed at the electrical ports. The matching layers are beneficial for increasing the total throughput of energy when compared to an unmatched transducer structure. The aluminium layer is used for mounting, therefore the center of structure resists motion along any direction.

To sum up, the proposed structure can be explained as an acoustic transducer that uses another one for its backing property. The transducer structure provides capability of being used without any air – backing material that narrows the communication area to a half – space. The proposed structure provides full space communication. It is suitable for new communication techniques, such as spread spectrum applications, at short distances. When applied at high frequency range, it provides advantages like low power emission, and hence undetectability at a distance, as well as suitability for networking. The proposed design introduces new features for wideband transducer applications where the physical achievable dimension of transducers has always introduced tremendous barriers.

1.6 Organization of the Thesis

Chapter 2 introduces the analogy between acoustics and electromagnetics besides microwave theory. The general boundary conditions are discussed.

Chapter 3 summarizes several characteristics of transducers. We discuss the affects of backing materials; besides benefits of using quarter – wavelength matching layers.

Chapter 4 introduces the proposed wideband bi – directional transducer model. We discuss the transmitting and receiving modes of the proposed model.

Chapter 5 gives the propagation characteristics of a wave in underwater media. We discuss the propagation of a wave towards the half – space of the receiving transducer; the sensed acoustic forces on two acoustic ports of the receiver and the generated voltage at each electrical port.

Chapter 6 discusses the characteristics of the proposed transducer for several occasions based on the orientation of receiver and transmitter in underwater media.

The results of wideband bi – directional transducer structure on several studies are presented in Chapter 7. We also discuss future work that can be done to identify the potential of the proposed transducer structure.

Chapter 2

Analogy between Acoustics and Electromagnetics

The wave properties of acoustics can be analyzed in a similar way with electromagnetic waves. This chapter details the analogy between acoustics and electromagnetics.

2.1 Wave Characteristics

Acoustics is the science of compressive waves in solids, liquids, or gases. There are two types of acoustic waves: (i) The longitudinal waves; the motion of a particle is in the same direction with the force applied to it. As a result, a force that is applied to the acoustic medium causes the medium to expand or contract in the same direction of it. (ii) The shear waves; the motion of the particle is transverse to the direction of force applied to it. Solids are subject to both shear and longitudinal waves; fluids do not support shear stress. Hence, throughout the thesis, we are concerned with only the longitudinal waves.

There are two fundamental differential equations for acoustic waves, based on conservation of mass and equation of motion.

Conservation of Mass: The relation between the particle velocity $\overline{v}$ and instantaneous density ρ_m is needed to be detailed in order to derive the relation of motion of the fluid with respect to its compression or expansion. For a volume of

element, the net rate at which mass flows into the volume through its surface must equal the rate at which the mass within its volume increases:

$$\frac{\partial \rho_m}{\partial t} + \nabla \cdot (\rho_m \vec{v}) = 0 . \qquad (2.1)$$

We consider that ρ_m equals $\rho_{m0} + \rho_{m1}$, where ρ_{m0} is the unperturbed density and ρ_{m1} is the perturbation in the density. We assume that the direction of propagation and hence the displacement of material is in z direction. Assuming that $\vec{v}$ and ρ_{m1} are first order perturbations, and keeping only first terms:

$$\rho_{m0} \frac{\partial \vec{v}}{\partial z} + \frac{\partial \rho_m}{\partial t} = 0 , \qquad (2.2)$$

where $\rho_m = \rho_{m0} + \rho_{m1} = \rho_{m0} / (1 + S) = \rho_{m0}(1 - S)$. Thus,

$$\frac{\partial \vec{v}}{\partial z} = \frac{\partial S}{\partial t} . \qquad (2.3)$$

S is the strain and proportional to stress $T = cS$, where c is the elastic constant of the material.

Equation of Motion: The equation of motion of a point in a material, when a small time – variable stress is applied, can be solved using Newton's second law. The net translational force per unit area applied to the material of length l is $l \partial T / \partial z$, so the equation of motion is:

$$\frac{\partial T}{\partial z} = \rho_{m0} \dot{v} = \rho_{m0} \frac{\partial v}{\partial t} . \qquad (2.4)$$

Wave Equation: We combine the two acoustic differential equations Eq (2.3) and Eq. (2.4). They lead to:

$$\frac{\partial^2 T}{\partial z^2} = \frac{\rho_{m0}}{c_s} \frac{\partial^2 T}{\partial t^2} . \qquad (2.5)$$

For a wave of radian frequency ω, with all field quantities varying as $\exp(j\omega t)$, the solution to Eq. (2. 5) is in the form $\exp[j(\omega t \pm \beta_a z)]$, where

$$\beta_a = \omega(\frac{\rho_{m0}}{c_s})^{1/2} = \frac{\omega}{V_a}, \tag{2. 6}$$

is the propagation constant and $V_a = (\frac{c_s}{\rho_{m0}})^{1/2}$ is the acoustic wave velocity. The velocity of sound is approximately 1500 m/s in water, and ~1500 – 13000 m/s in solids. Hard materials such as metals and ceramics have greater velocities.

The phase velocity for an acoustic wave is:

$$v_p = \omega / \beta_a = V_a, \tag{2. 7}$$

and the group velocity is:

$$v_g = 1/(d\beta_a / d\omega) = (c_s / \rho_{m0})^{1/2} = V_a, \tag{2. 8}$$

which are same in a non-dispersive medium.

Acoustic Impedance: In analogy to Electromagnetic theory, we can define the acoustic impedance (specific acoustic impedance) *Z* as,

$$Z = -\frac{T}{v}. \tag{2. 9}$$

The characteristic electromagnetic impedance Z_0 for air is ~377 ohms, while the acoustic impedance for air at 20^0 is ~415 [Ns/m^3-s] and for water at 20^0 is ~1.5 * 10^6 [Ns/m^3-s].

Eq. (2.3) and Eq. (2.4) can be rewritten as follows:

$$\frac{\partial \vec{v}}{\partial z} = j\omega S = \frac{j\omega T}{c}, \tag{2. 10}$$

and

$$\frac{\partial T}{\partial z} = j\omega\rho_{m0}v\,. \tag{2. 11}$$

These equations can be compared with the transmission line equations for voltage and current along a transmission line, which are;

$$\frac{\partial V}{\partial z} = -j\omega LI\,, \tag{2. 12}$$

and

$$\frac{\partial I}{\partial z} = -j\omega CV\,, \tag{2. 13}$$

where L is series inductance per unit length and C is the shunt capacitance per unit length. The propagation constant of a wave propagating along this line is $\beta_a = \omega\sqrt{LC}$ and its impedance is $Z_0 = \sqrt{L/C}$.

Comparing the equations (2.3, 2.4, 2.12 and 2.13), it is seen that *T* is analogous to *V* and *v* is analogous to *I*. Therefore, stress and particle velocity solutions can be written as follows for a uniform plane wave confined to z – axis propagation.

$$T = T_F e^{j(\omega t-\beta_a z)} + T_B e^{j(\omega t+\beta_a z)}\,, \tag{2. 14}$$

and

$$\vec{v}(z) = \overline{v}\hat{a}_z = \overline{v}_F e^{j(\omega t-\beta_a z)} + \overline{v}_B e^{j(\omega t+\beta_a z)}\,. \tag{2. 15}$$

Eq (2.5) can be compared with the electromagnetic wave equation solution of a source free region:

$$(\nabla^2 + w^2\mu_0\varepsilon_0)\overline{E} = 0\,, \tag{2. 16}$$

which gets use of Maxwell's equations:

$$\begin{aligned} \nabla\times\overline{E} &= -\mu_0\frac{\partial\overline{H}}{\partial t}, \\ \nabla\times\overline{H} &= \varepsilon_0\frac{\partial\overline{E}}{\partial t}. \end{aligned} \tag{2. 17}$$

Comparing the Maxwell's equations (Eq. 2.17) with Eq. (2.3 and 2.4), we conclude that velocity and stress, $\vec{v}$ and T are analogous to the electromagnetic field vectors, $\bar{E}$ and $\bar{H}$. The significant difference between electromagnetic and acoustic waves is their attitude with respect to the propagating waves. $\bar{E}$ and $\bar{H}$ are both orthogonal to the direction of propagation, whereas $\vec{v}$ is generally a vector parallel to the direction of propagation and T is a scalar function of position. As a result, there is no polarization of acoustic waves, as there exists for electromagnetic waves.

2.2 Power and Energy

Acoustic power and energy definitions are similar to electromagnetic implementations. For a uniform plane wave in the time domain, *acoustic power density*, or intensity is:

$$I_s(t) = p(t)v(t) = p^2 / Z[Wm^{-2}]. \tag{2. 18}$$

The intensity of a uniform electromagnetic plane wave in the time domain is:

$$I(t) = E(t)H(t) = E^2 / Z_0[Wm^{-2}]. \tag{2. 19}$$

2.3 Boundary Conditions

There are two acoustic boundary conditions to be satisfied for all times at all points on the boundary: (i) The acoustic pressures on both sides of the boundary must be equal and (ii) normal components of the particle velocities on both sides of the boundary must be equal.

For electromagnetic at every boundary: (i) The tangential component of electric field must be continuous across an interface and (ii) the normal component of magnetic field across an interface between two media must be continuous**.**

2.3.1 Green's function

Green's function is used to solve partial differentiation equations of electromagnetics and acoustics. The Green's function is a technique to the solution of the partial differentiation equation that is obtained using a unit source (Impulse, Dirac Delta) as the driving function. The solution to the driving force is written as a superposition of the impulse response solutions (Green's function) with the Dirac delta source at different locations, which in the limit reduces to an integral. The Green's function, $G = \frac{Ae^{-jkR}}{R}$ is a solution to the wave equation for a source point at x', y', z':

$$\nabla^2 G + k^2 G = \delta(x - x', y - y', z - z')\text{.} \tag{2. 20}$$

The derivation of Green's function is as described in Appendix I.

Green's theorem is useful to find a solution for the potential at a point due to excitation by a transducer. This is equivalent to finding the general solution for ϕ at any point, given ϕ and $\nabla\phi$ on a surface surrounding the point x, y, z. We multiply the wave equation

$$\nabla^2 \phi + k^2 \phi = 0\text{ ,} \tag{2. 21}$$

with G and multiply the Green's function wave equation with ϕ.

$$G\nabla^2 \phi + k^2 \phi G = 0\text{ ,} \tag{2. 22}$$

$$\phi\nabla^2 G + k^2\phi G = \phi\delta(x-x', y-y', z-z')\,. \tag{2. 23}$$

After subtracting Eq. (2.22) from Eq. (2.23), we integrate the resulting expression over volume *V,* and obtain:

$$\begin{aligned}\phi(x,y,z) &= \int_{V'}(\phi\nabla'^2 G - G\nabla'^2\phi)dV',\\ \phi(x,y,z) &= \int_{V'}\nabla'\bullet(\phi\nabla' G - G\nabla'\phi)dV'.\end{aligned} \tag{2. 24}$$

where the superscript indicates that the integration is done with respect to x', y', z' variables. Applying Gauss's theorem to the integral reduces the equation to:

$$\phi(x,y,z) = \int_{s'}(\phi\nabla' G - G\nabla'\phi)\bullet \mathrm{n}\, ds'\,, \tag{2. 25}$$

where s' is any point enclosing the point x, y, z and **n** is outward normal from the volume *V.* As a result, ϕ can be determined at any point if we know ϕ and $\nabla\phi$ on the surrounding surface. This statement is also known as *Helmholtz's integral theorem.*

We assume that a piston transducer of area S_1 is in a baffle of area S_2 and the rest of the enclosing surface volume is $\sum$ and R$\rightarrow\infty$ as z $\rightarrow\infty$. When R$\rightarrow\infty$, both ϕ and $G \rightarrow \frac{e^{-jkR}}{R}$. This cancels out the two terms in the integral Eq. (2.23). *Sommerfeld Radiation condition* makes the assumption of ignoring contributions to the integral from the surface at infinity. We can write the general Green's function as

$$\phi(x,y,z) = \int_{s_1}(\phi\nabla' G - G\nabla'\phi)\bullet \mathrm{n}\, ds'\,, \tag{2. 26}$$

where **n** is the normal pointing into the area of transducer and S_1 is the area of transducer.

Eq. (2.24) can be simplified depending on the boundary conditions of ϕ and G and their derivatives on S_1.

The most obvious way to simplify a solution for the equation is either to have $G=0$ or $\partial G/\partial z$ on the transducer and its baffle. Therefore, we only need to indicate $\partial\phi/\partial z$ or ϕ on the transducer. There are two specific boundaries that can be used based on the general Green's function:

1) Rigid Baffle
2) Pressure Release Baffle

For both cases, we assume there exists a source $\delta(x-x',y-y',z-z')$ and its image $\delta(x-x',y-y',z+z')$ with respect to the plane $z=0$.

2.3.2 Rigid Baffle

The Green's function can be written as following for a Rigid Baffle:

$$G=-\frac{1}{4\pi}\left(\frac{e^{-jkR_1}}{R_1}+\frac{e^{-jkR_2}}{R_2}\right), \tag{2.27}$$

where

$$\begin{aligned} R_1&=\sqrt{(z'-z)^2+(x'-x)^2+(y'-y)^2},\\ R_2&=\sqrt{(z'+z)^2+(x'-x)^2+(y'-y)^2}. \end{aligned} \tag{2.28}$$

This yields a solution for the potential at any point ($z\geq 0$) in the form of:

$$\phi(x,y,z) = \frac{1}{2\pi}\int_s u_z(x',y',0)\frac{e^{-jkR}}{R}ds', \qquad (2.\ 29)$$

where u_z is the particle displacement along z – axis and $u = \nabla\phi$.

The Green's function for Rigid baffle suits the boundary condition $\partial G/\partial z' = 0$ at $z' = 0$. It specifies that there is no motion on the baffle and the normal component of the particle velocity is zero. If an acoustic wave impinges on the boundary, it completely reflects back. The given example is analogous to a dielectric boundary.

A rigid baffle is also analogous to an open circuited transmission line, such as the reflection coefficient on the baffle equals +1.

2.3.3 Pressure Release Baffle

For Pressure Release Baffle the Green's function becomes:

$$G = -\frac{1}{4\pi}\left(\frac{e^{-jkR_1}}{R_1} - \frac{e^{-jkR_2}}{R_2}\right). \qquad (2.\ 30)$$

This yields a solution for the potential at any point ($z \geq 0$) in the form

$$\phi(x,y,z) = \frac{jk}{2\pi}\int_s \phi(x',y',0)\frac{e^{-jkR}(1+1/jkR)\cos\theta}{R}ds', \qquad (2.\ 31)$$

where θ is the angle between the radius **R** and the z axis.

The Green's function for Pressure Release baffle suits the boundary condition $G = 0$ at $z' = 0$. It specifies that the pressure on both sides of the boundary is equal. The given example is analogous to a conducting boundary.

A pressure release baffle is also analogous to a short circuited transmission line, such that the reflection coefficient on the baffle equals -1.

Chapter 3

Acoustic Underwater Transducer

Electromechanic transducers convert electrical energy into mechanical energy and vice versa. Therefore, they are used to transmit and receive media via acoustic waves in underwater.

3.1 Mason's Model

In Figure 3. 1, we consider a uniform transducer whose length, l is greater than its wavelength, λ and its electrodes on opposite surfaces are parallel to the z direction. We assume that E_x and E_y are zero, since the electrodes short out the field.

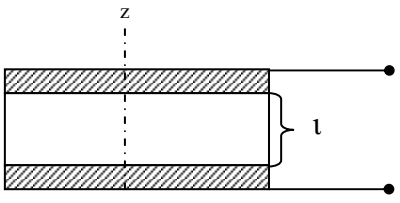

Figure 3. 1. Piezoelectric resonator of length ι with electrodes on opposite surfaces.

The piezoelectric transducer can be regarded as a three port black-box (Figure 3. 2) having two acoustic ports and an electrical port.

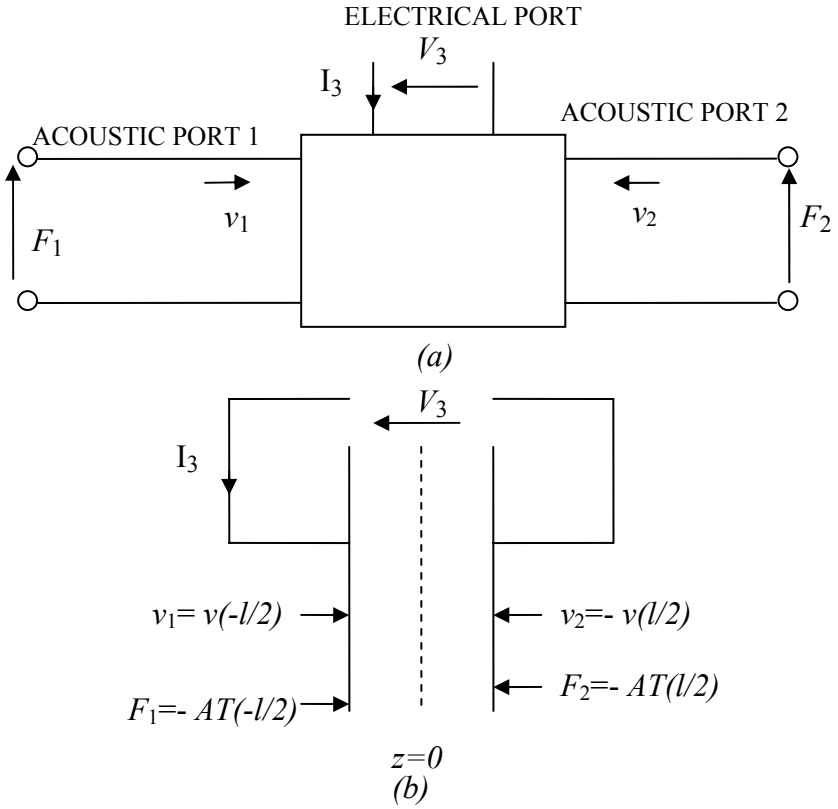

Figure 3. 2. (a) Transducer, regarded as a three – port black box, (b) The force and particle velocity notation on the transducer.

The force and particle velocity are similar to voltage and current for the electrical circuits. The external force that is applied to the piezocomposite material is

$$F = -AT\,, \tag{3. 1}$$

where A is the surface area of the transducer and T is the internal stress. The boundary conditions at the acoustic ports are:

$$\begin{aligned} F_1 &= -AT(-l/2), \\ F_2 &= -AT(l/2), \\ v_1 &= v(-l/2), \\ v_2 &= -v(l/2). \end{aligned} \tag{3. 2}$$

We use Eq. (2.14) and Eq. (2.15) to derive the frequency domain equations for stress and velocity, where:

$$v = v_F e^{-j\beta_a z} + v_B e^{j\beta_a z}, \tag{3. 3}$$

and

$$T = T_F e^{-j\beta_a z} + T_B e^{j\beta_a z} - hD. \tag{3. 4}$$

The following matrix is the general solution for a three port transducer:

$$\begin{bmatrix} F_1 \\ F_2 \\ V_3 \end{bmatrix} = -j \begin{bmatrix} Z_C \cot \bar{\beta}_a l & Z_C \operatorname{cosec} \bar{\beta}_a l & \frac{h}{w} \\ Z_C \operatorname{cosec} \bar{\beta}_a l & Z_C \cot \bar{\beta}_a l & \frac{h}{w} \\ \frac{h}{w} & \frac{h}{w} & \frac{1}{wC_0} \end{bmatrix} \begin{bmatrix} v_1 \\ v_2 \\ I_3 \end{bmatrix}, \tag{3. 5}$$

where the clamped (zero strain) capacitance of the transducer is:

$$C_0 = \frac{\varepsilon^S A}{l}. \tag{3. 6}$$

Derivation of Mason's Matrix is detailed in Appendix II.

We define the acoustic impedance of the piezocomposite material with surface area A, as:

$$Z_c = Z_0 A \text{ [kg/s]}, \tag{3. 7}$$

and

$$Z_0 = \rho_0 c_0 \text{ [kg/m}^2\text{-s]}, \tag{3. 8}$$

where ρ_0 is the density of piezocomposite material and c_0 is the velocity of sound as defined in Chapter 2. Z_c is also called the *radiation impedance.*

The Matrix given in Eq. (3.5) leads to the Mason circuit shown in Figure 3. 3. The right-hand and left-hand sides of the transducer circuit model are similar to each other with the exception of an extra potential hI_3 / jw which is in series with the potentials generated by v_1 and v_2. The circuit is analogous to a transmission line if we assume that there is no net current through the electrical port. The transducer model employs a transformer, with transformer ratio:

$$N = hC_0 = \frac{eC_0}{\varepsilon^s} = \frac{eA}{l}[C/m]. \tag{3. 9}$$

The ratio $\frac{V_3}{I_3} = Z_3$ gives the input impedance of the transducer that can be find by using the boundary conditions and the transducer matrix.

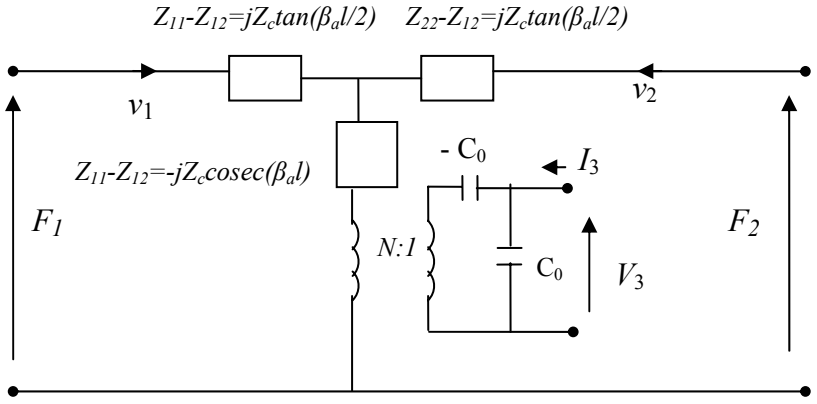

Figure 3. 3. Mason series equivalent circuit.

3.2 An Air-Backed Transducer in Air

We derive the properties of an air-backed and unloaded transducer in air. If we assume that acoustic port 1 provides the backing for the transducer and acoustic port 2 is in air then the impedances of acoustic ports are $Z_1 = Z_2 = 0$ and $F_1 = F_2 = 0$. The electrical equivalent circuit of the transducer is sketched in Figure 3. 4. where:

$$\begin{aligned} Z_b &= jZ_c \tan(\beta_a l), \\ Z_a &= -jZ_c \cos ec(\beta_a l). \end{aligned} \tag{3. 10}$$

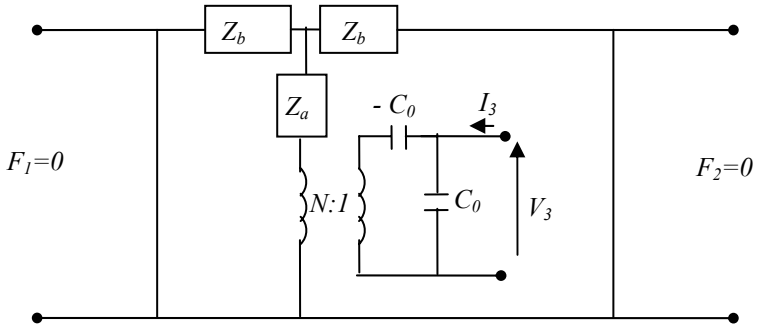

Figure 3. 4. Electrical circuit of an air-backed and unloaded transducer in air.

We use the Mason's Matrix and derive the input impedance of the transducer as:

$$Z_3 = \frac{V_3}{I_3} = \frac{1}{jwC_0}(1 - k_T{}^2 \frac{\tan \bar{\beta}_a l/2}{\bar{\beta}_a l/2}), \tag{3. 11}$$

where k_T is the piezoelectric coupling constant for a transversely clamped material; for PZT-5A, k_z^2 is 0.33.

Eq. (3.11) shows that Z_3 can be assumed as a capacitor C_0 in series with motional impedance, Z_a:

$$Z_a = -\frac{k_T{}^2}{jwC_0}\frac{\tan \bar{\beta}_a l/2}{\bar{\beta}_a l/2}. \qquad (3.12)$$

The transducer introduces a parallel resonance with infinite electrical impedance. The transducer can be modeled as an inductance and capacitance in parallel at odd numbers of half – wavelengths long of transducer, where $\bar{\beta}_a l = (2n+1)\pi$. The corresponding resonance frequency is given by the relationship:

$$\omega_n = \frac{(2n+1)\pi V_a}{l}. \qquad (3.13)$$

The transducer introduces zero electrical impedance at a frequency near ω_0. The transducer behaves like a capacitance and inductance in series. The input impedance of the transducer is zero at frequency ω_1, where:

$$\frac{\tan \bar{\beta}_a l/2}{\bar{\beta}_a l/2} = \frac{1}{k_T{}^2}. \qquad (3.14)$$

We consider the length of the transducer as half – wavelength long, and the resonance frequency of a half – wavelength transducer f_0 is 400 kHz. The density of the ceramic material is 2650 kg/m^3 and velocity of sound, c_c equals 4600 m/sec. The surface area, A of the square shaped layer is 9*10^{-6} m^2. The radiation impedance of the ceramic $Z_c = A\rho_c c_c$ is 109.8 kg/s, where $\rho_c c_c$ = 12.2*10^6 kg/m^2-s. The wavelength of ceramic layer, $\lambda_c = \frac{c_c}{f_0}$ at the resonance frequency equals 0.015 m. Its propagation constant $\bar{\beta}_a = \frac{2\pi}{\lambda_c}$ is 418.9 at f_0. The plot of

normalized admittance versus normalized frequency is sketched in Figure 3. 5. The susceptance seen at the input port is infinite at the resonance frequency.

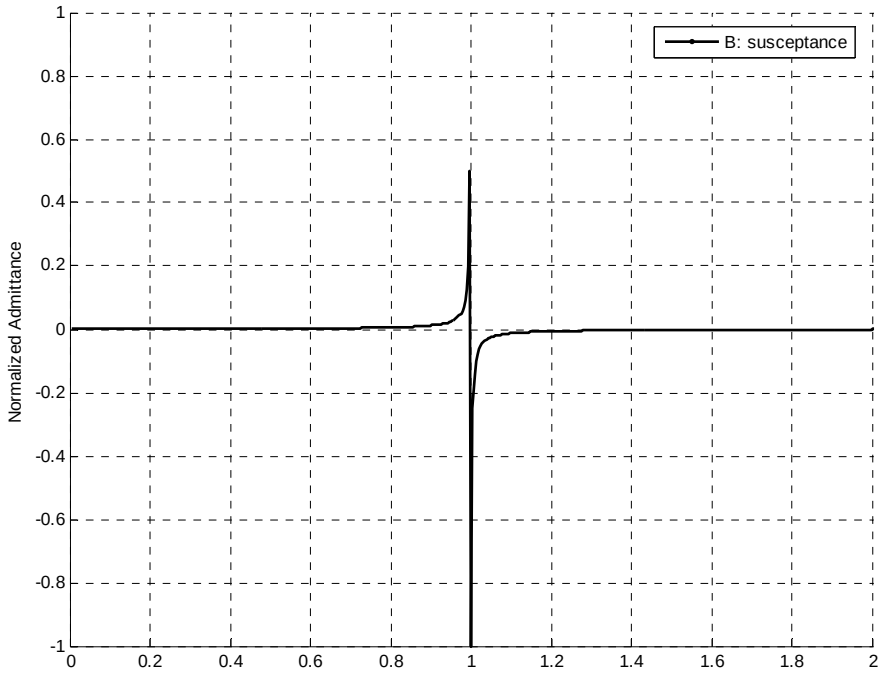

Figure 3. 5. Normalized admittance versus normalized frequency graph for an air – backed and unloaded transducer in air.

3.3 An Air - Backed Transducer in Water

The air - backed half – wavelength long transducer is placed with its front surface in water. The impedance of water acts as load introduced to the front acoustical surface of the transducer, where $Z_1 = 0$ and $Z_2 = Z_w$. The radiation impedance of water is 13.5 kg/s, the density of water ρ_w equals 1000 kg/m^3, velocity of sound c_w is 1500 m / sec and $A = 9*10^{-6}$ m^2. The acoustic impedance of transducer is greater compared to the acoustic impedance of water.

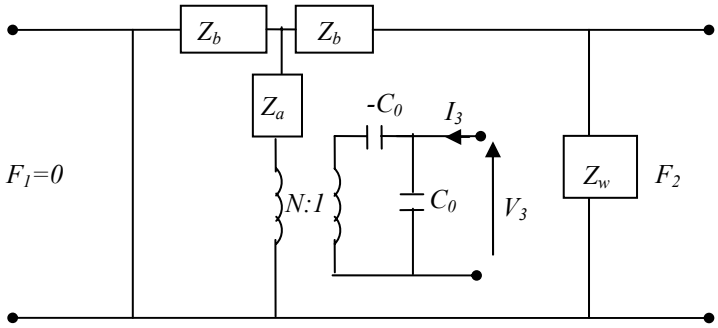

Figure 3. 6. Electrical circuit of an air-backed and transducer immersed in water.

We derive the input impedance of the air - backed half – wavelength long transducer immersed in water at its resonance frequency using the matrix given in Eq. (3.5), where:

$$Z_3 = \frac{4k_T{}^2}{\pi\omega_0 C_0}\frac{Z_c}{Z_w}. \qquad \textbf{(3. 15)}$$

The normalized admittance versus normalized frequency is as sketched in Figure 3. 7. Its susceptance is zero at the resonance frequency of a half – wavelength long transducer. The real part of the function is symmetric around its resonance frequency.

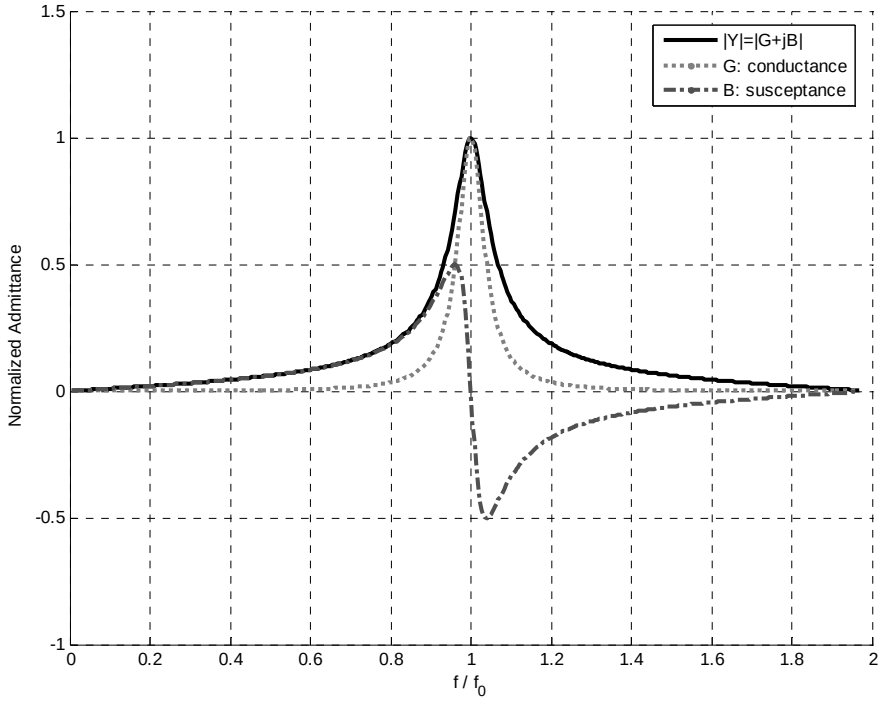

Figure 3. 7. Normalized admittance versus normalized frequency for air – backed transducer immersed in water.

If the transducer structure is replaced with another one that has lower acoustic impedance, then the input impedance (Eq. 3.15) decreases and the 3 dB effective bandwidth of the transducer to increase. We demonstrate the change of the admittance response of transducer with respect to changes in acoustic impedance of transducer when the transducer structure is immersed in water, in Figure 3. 8 and Figure 3. 9. The bandwidth of the conductance increases when the impedance of transducer becomes close to the impedance of water (Figure 3. 8). For $Z_w = 1/\sqrt{2}Z_c$ the admittance response of transducer is flat. When $Z_w > 1/\sqrt{2}Z_c$ there are peaks on both sides of f_0. There is a sharp response near $f=f_0$ as the acoustic impedance of transducer is increased. When Z_w / Z_c is very large the peaks tend to occur at $f=0.5f_0$ and $f=1.5f_0$. The susceptance at the resonance frequency is not affected from changing the characteristic impedance; it is zero for all values (Figure 3. 9).

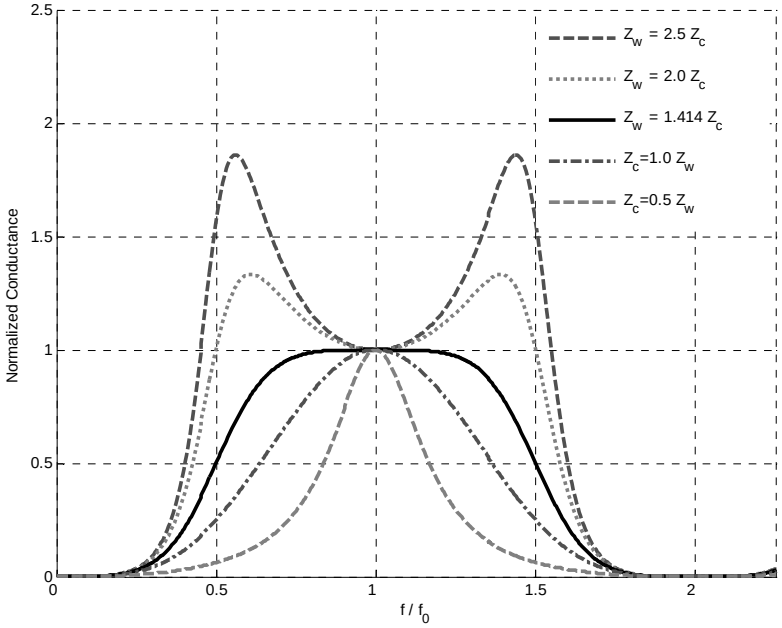

Figure 3. 8. Normalized conductance versus normalized frequency for an air – backed transducer immersed in water with changing impedance of transducer.

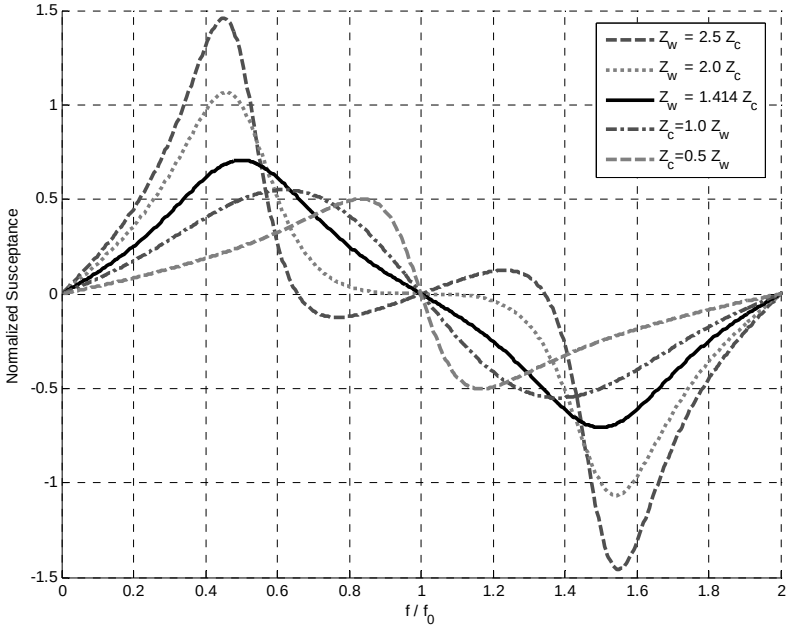

Figure 3. 9. Normalized susceptance versus normalized frequency for an air – backed transducer immersed in water with changing impedance of transducer.

We feed the transducer with unit impulse via its electrical port, V_3 (Figure 3. 6). The transfer function F_2 / V_3 of the radiating acoustic port is examined. F_2 is the force generated at the receiving acoustic port and V_3 is the voltage at the transmitting electrical port. The transfer function is as depicted in Figure 3. 10. The 3 dB effective bandwidth of the function is 12%. Its effective resonance frequency is less than the resonance frequency of a half – wavelength ceramic layer. This is due to the effect of negative capacitance, $-C_0$.

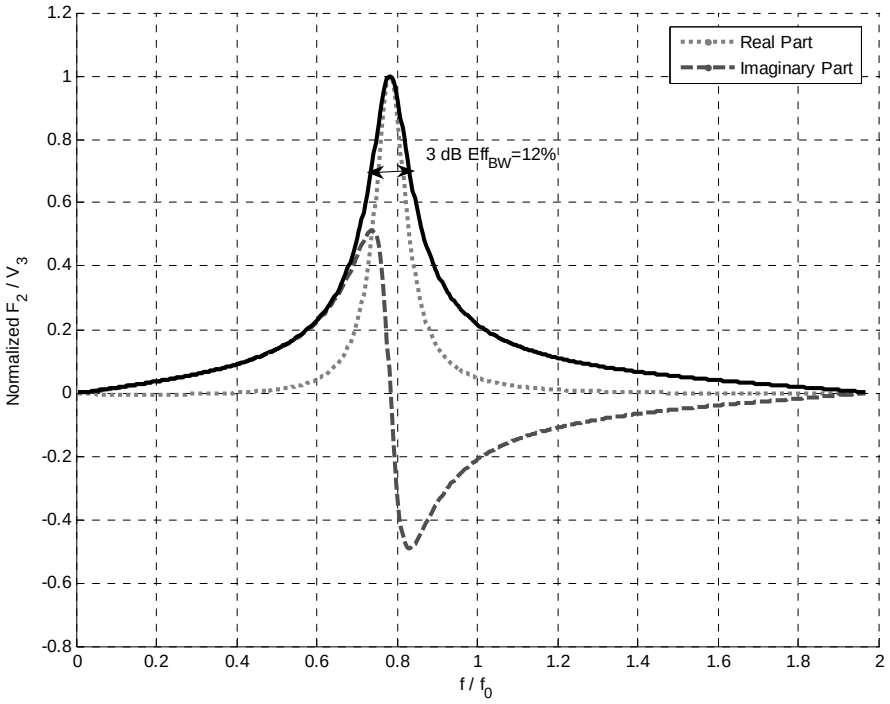

Figure 3. 10. Normalized transfer function of an air – backed transducer immersed in water; F_2 / V_3, where $Z_1 = Z_{water}$, $Z_2 = 0$ and 3 dB Eff_{BW}=12%.

Instead of using an air-backing material at the acoustic port 1 (Figure 3. 6), we adjust a quarter – wavelength layer whose impedance equals to the radiation impedance of water, $Z_1 = 13.5\,kg/s$. When a unit impulse is radiated from the electrical port of the transducer, the transfer function of force generated on an acoustic port F_2, F_2 / V_3, becomes as depicted in Figure 3. 11. The magnitude of the transfer function is less than that of an air – backed transducer immersed in water

(Figure 3. 10). However, its 3 dB effective bandwidth is greater than the air – backed transducer, it is 23 %.

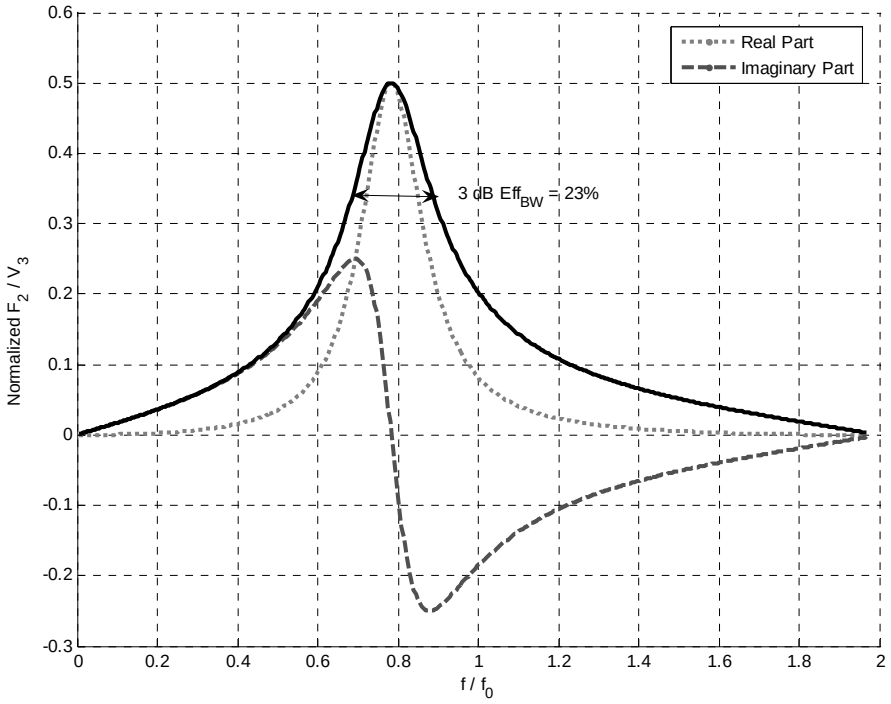

Figure 3. 11. Normalized transfer function of a transducer with backing material immersed in water; F_2 / V_3 where $Z_1 = Z_2 = Z_{water}$, 3 dB Eff_{BW}=23%.

3.4 Transducer with Matching Layers

We assume that both sides of the transducer are terminated with quarter wavelength matching layers. The transducer is immersed in water, $Z_1=Z_2 = Z_{water}$. The equivalent Mason circuit is as depicted in Figure 3. 12.

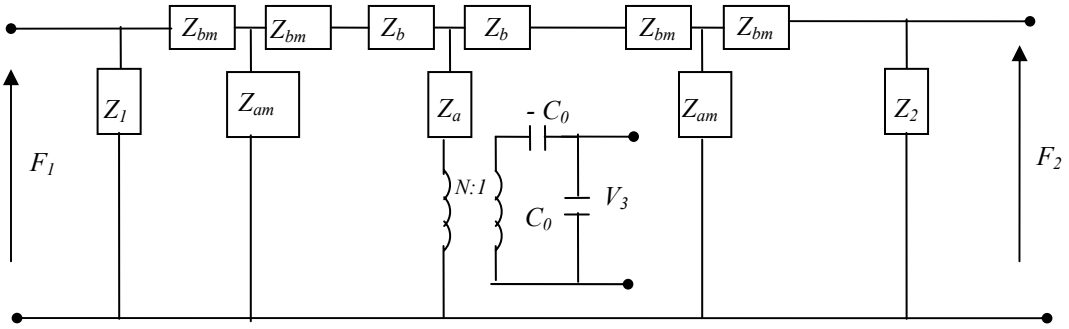

Figure 3. 12. Transducer immersed in water with matching layers.

We demonstrate the impedance values of matching layers with Z_{am} and Z_{bm} abbreviations, where:

$$\begin{aligned} Z_{bm} &= jZ_m \tan(\beta_m l_m / 2), \\ Z_{am} &= -jZ_m \operatorname{cosec}(\beta_m l_m), \end{aligned} \qquad (3.16)$$

and

$$\begin{aligned} Z_m &= A\rho_m c_m, \\ \lambda_m &= \frac{C_m}{f}, \\ \beta_m &= \frac{2\pi}{\lambda_m}. \end{aligned} \qquad (3.17)$$

the radiation impedance of matching layer is $Z_m = 27\,kg/s$. ρ_m equals 3000 kg/m^3 and c_m equals 1000 m/s. The wavelength of the matching layer, λ_m is 0.0025 m at the resonance frequency of a half – wavelength ceramic, f_0 = 400 kHz. Its length, $l_m = \frac{\lambda_m}{4}$ is 0.625 mm. The propagation constant β_m equals 2.51*10^3.

The admittance realized right after the transformer is shown in Figure 3. 13. The function employs two symmetric peaks. The transducer is much more

effective compared to the transducer immersed in water with no matching layers. The matching layers improve the bandwidth of admittance function.

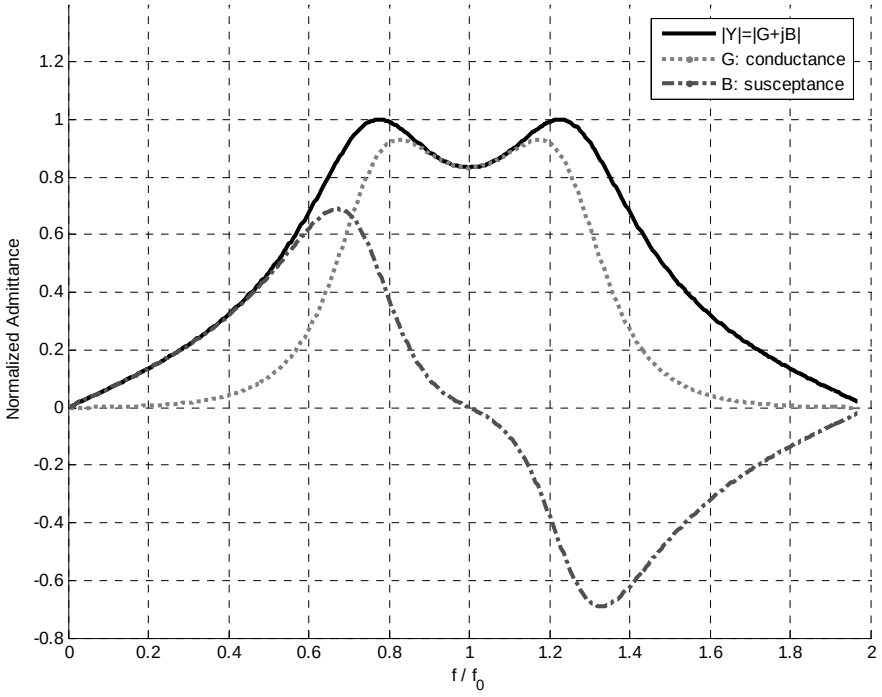

Figure 3. 13. Normalized admittance versus normalized frequency of a transducer matched to water $Z_1=Z_2 = Z_{water}$.

We demonstrate the effect of decreasing the acoustic impedance of matching layers, Z_m in Figure 3. 14. The impedance graphs are sketched for 100%, 95%, 90%, 83%, 75% and 65% values of Z_m. The normalized admittance value seen from the electrical ports at the resonance frequency, f_0 increases as Z_m decreases. On the other hand, the effective frequency band remains unchanged as the acoustic impedance of matching layer decreases. The admittance has only one peak at the resonance frequency f_0, when the matching layer acoustic impedance values are greater than 83%. For 83% Z_m, the admittance response of transducer is flat. There are two peaks on both sides of f_0 for acoustic impedance of matching layers greater than 83% Z_m.

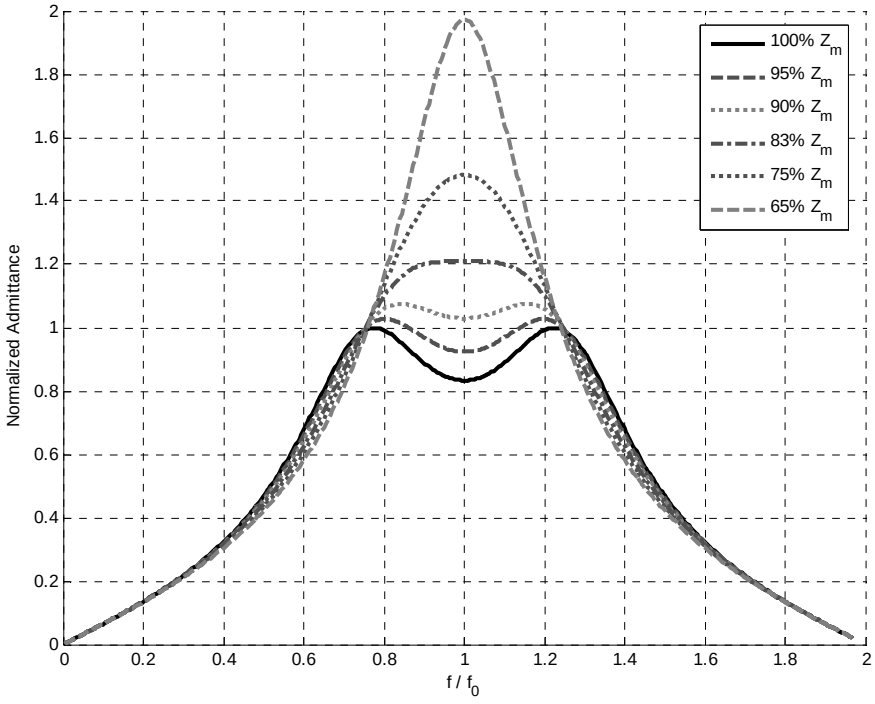

Figure 3. 14. Normalized admittance versus normalized frequency plots for a matched transducer with decreasing $Z_{m.}$

We demonstrate the effect of increasing the impedance of matching layers, Z_m in Figure 3. 15. The impedance graphs are sketched for 100%, 105%, 110%, 115%, 120% and 145% values of Z_m. The normalized admittance value seen from the electrical ports at the resonance frequency, $f_{0,}$ decreases as the percentage of Z_m increases. The peaks tend to move away from the resonance frequency as Z_m increases.

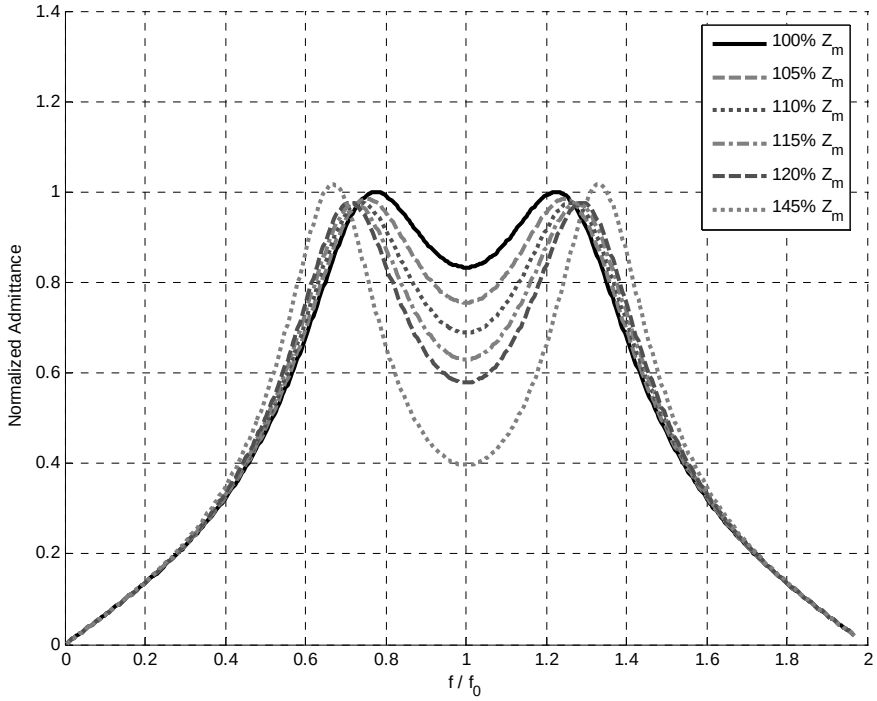

Figure 3. 15. Normalized admittance versus normalized frequency plots for a matched transducer with increasing $Z_{m.}$

We demonstrate the effect of decreasing the length of matching layers, l_m in Figure 3. 16. The impedance graphs are sketched for 100%, 95%, 90%, 85%, 80% and 65% values of l_m where l_m =625 μm. When the length of admittance layer is less than 80% l_m, the admittance has only one peak, which occurs below the resonance frequency $f_{0.}$ The peak moves towards the resonance frequency, $f_{0,}$ as the length of matching layer is decreased further. The admittance at the resonance frequency, f_0 increases as the length of matching layer decreases.

We demonstrate the effect of increasing the length of matching layers, l_m in Figure 3. 17. The impedance graphs are sketched for 100%, 105%, 110%, 115%, 120% and 130% values of $l_{m.}$ The admittance tends to have only one peak as the length of matching layer increases besides the peak occurs above, f_0. The peak moves towards the resonance frequency $f_{0,}$ as the length of matching layer is increased. The admittance increases as the length of matching layer increases.

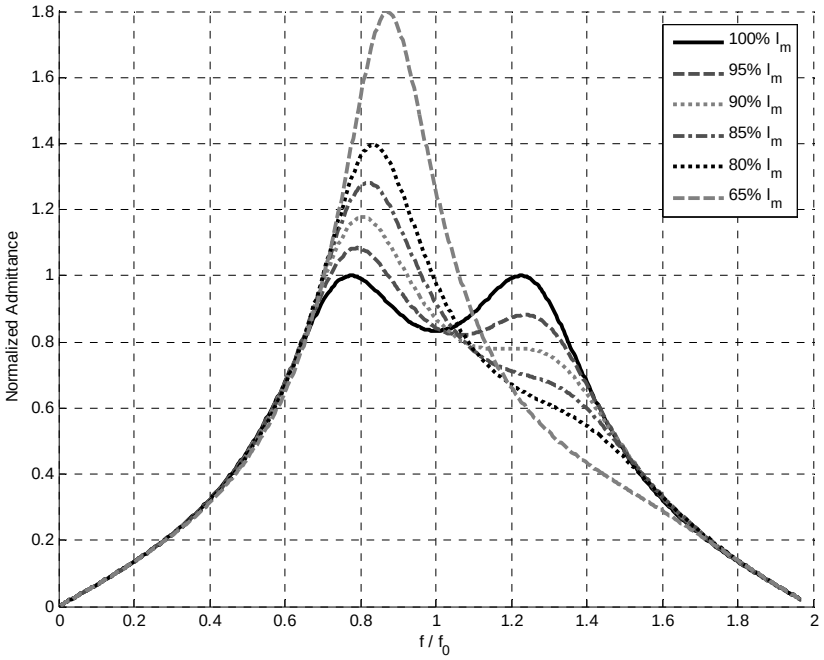

Figure 3. 16. Normalized admittance versus normalize frequency plots for a matched transducer with decreasing l_m.

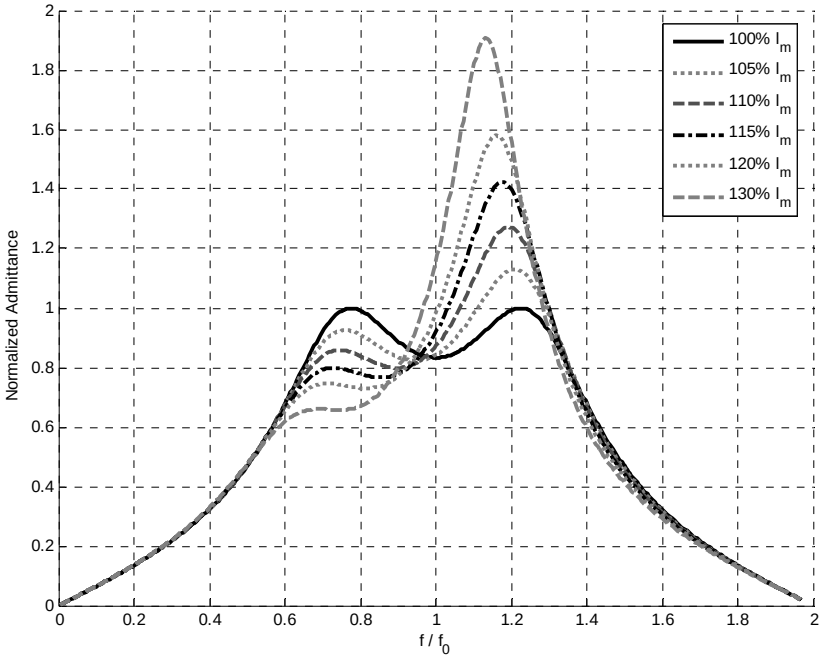

Figure 3. 17. Normalized admittance versus normalize frequency plots for a matched transducer with increasing l_m.

Chapter 4

Wideband Bi – Directional Composite Piezoelectric Transducer

The proposed transducer structure has a wide bandwidth; besides it can be used to receive and send acoustic waves to the two half – spaces orthogonal to its radiating faces. This chapter details the characteristics of receiving and transmitting modes of the transducer.

4.1 Properties

The proposed transducer structure is composed of matching, aluminium and 1 - 3 composite ceramic layers as shown in Figure 4. 1. The layers are square shaped; having surface area, $A = 9*10^{-6}$ m^2. The two radiating faces (to each half space) of the transducer are displaced by the length of the structure. The displacement is about 2 wavelengths in water at resonance frequency, with available materials. The proposed transducer employs two electrical ports, V_1 and $V_{2;}$ besides two acoustic ports, F_1 and F_2 as depicted in Figure 4. 2.

The transducer structure has two back-to-back quarter wavelength thick 1 - 3 composite piezoelectric elements at its resonance frequency. Each element provides the *rigid*, or high impedance backing to the other element, maintaining efficiency. The structure has advantages compared to a half - wavelength

transduction element, such as; the acoustic forces received on two acoustic ports can be used to derive constructive linear combinations of two signals.

The ceramic layers are separated by a thin aluminium layer as shown in Figure 4. 1. The aluminium layer is not required from the performance point of view but it is included to provide a mounting support. Thus, the interface between two ceramic elements is a stress node.

We use quarter wavelength matching layers to match each piezocomposite layer to water. Acoustic matching provides the expected wide bandwidth to each element.

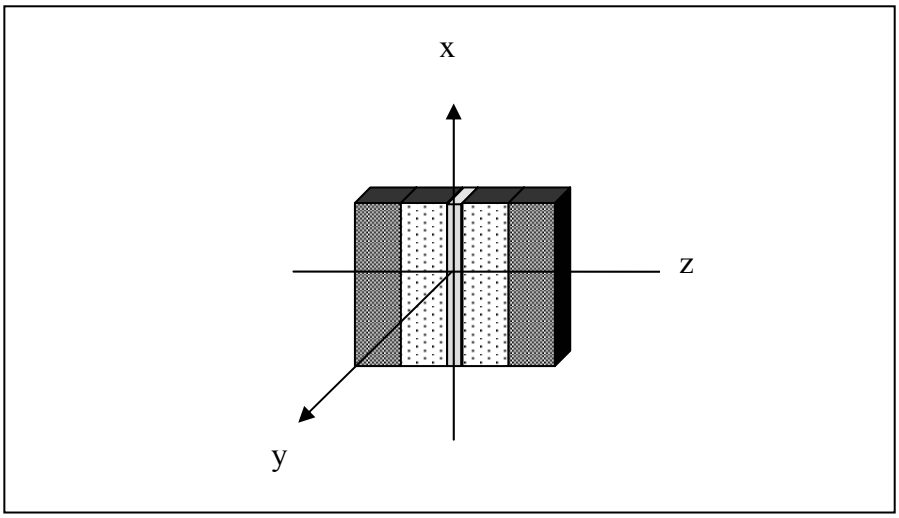

Figure 4. 1. Transducer structure made of 1 – 3 composite ceramic, matching and aluminium layers, where dark layers represents quarter – wavelength long matching layers, dotted layers are quarter – wavelength long composite piezoelectric layers and the middle thin layer is the aluminium.

The equivalent electrical model of the transducer is shown in Figure 4. 2. Ceramic layers are modeled using Mason's circuit model. The Mason's equivalent model of 1 - 3 composite ceramic layer includes the transformer ratio *'N'* as stated in Eq (3.9) where,

$$N = \frac{eA}{l} \approx 0.017[kg/m^2 s] = [C/m], \qquad e = 5.3 C/m^2. \tag{4. 1}$$

We sketch the aluminium and matching layers with their transmission line equivalent models.

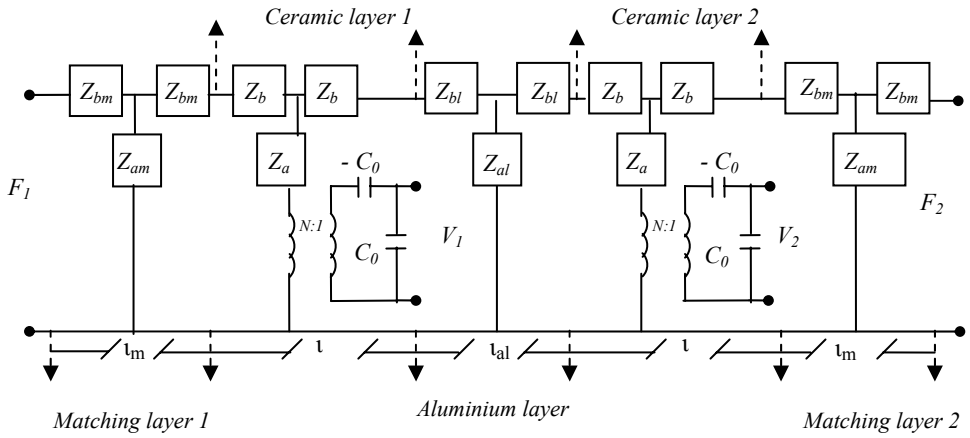

Figure 4. 2. Equivalent electrical model of proposed transducer structure.

We use 30% PZT-5A and 70% stycast for the 1 – 3 piezocomposite layers [13]. The layers are each $\lambda/4$=2.875 mm long, where $\lambda = c/f_0$ and f_0 is the resonance frequency of a half - wavelength transducer, 400 kHz. The characteristic impedance of each composite piezoelectric layer is $12.2*10^6 kg/m^2 s$. The wave velocity in the composite material *c* equals 4600 m/sec. Table I gives detailed data describing the properties of composite PZT-5A and stycast. Using the properties of piezocomposite layer, the clamped capacitance, C_0 is calculated to be7.2 pF.

The aluminium layer is 1 mm thick. The layer has characteristic impedance of 16.2 $*10^6 kg/m^2 s$. The wave velocity of the aluminium layer is 6000 m / sec and its density is 2700 kg / m^3.

The transducer structure is about 8 mm long at the resonance frequency of a half – wavelength transducer, f_0.

Table II presents detailed information about the transducer layers. The values reflect their figures at 400 kHz.

	TABLE 1 COMPOSITE PZT-5A and STYCAST PROPERTIES	
	PZT-5A	Stycast
Relative dielectric constant, free	$\frac{\varepsilon_{33}^{T}}{\varepsilon_0} = 1700$	
Relative dielectric constant, clamped	$\frac{\varepsilon_{33}^{S}}{\varepsilon_0} = 850$	
Elastic Stiffness	$c_{33}^{D} = 14.7 * 10^{10} N/m^2$ $c_{33}^{S} = 11.1 * 10^{10} N/m^2$	$c_S = 7.66 * 10^9 N/m^2$
Frequency Constant of a thin plate	$N_{3t} = 1890(Hz.m)$	
Acoustic wave velocity	$V_l = 4350 m/sec$	$V_l = 2750 m/sec$
density	$\rho = 7750 kg/m^3$	$\rho = 1160 kg/m^3$
Piezoelectric constant	$e_{33} = 15.8 C/m^2$	
Characteristic Impedance	$Z_c = 33.7 * 10^6 kg/m^2 - s$	$Z_s = 3 * 10^6 kg/m^2 - s$

Permittivity of free space is $\varepsilon_0 = 8.85 * 10^{-12} F/m$.

	TABLE 2 TRANSDUCER COMPONENTS		
	Matching layer	Piezocomposite layer	Aluminium layer
Surface Area	$A = 9*10^{-6} m^2$	$A = 9*10^{-6} m^2$	$A = 9*10^{-6} m^2$
Length	$l_m \approx 625 \mu m$	$l = 2.875 mm$	$l_{al} = 1.0 mm$
Wavelength	$\lambda_m = 2.5 mm$	$\lambda = 11.5 mm$	$\lambda_{al} = 15.0 mm$
Propagation constant	$\beta_m = 2.51*10^3$	$\beta = 546.4*10^3$	$\beta_{al} = 418.9*10^3$
Density	$\rho_m = 3000 kg/m^3$	$\rho = 4600 kg/m^3$	$\rho_{al} = 2700 kg/m^3$
Bulk velocity of sound	$c_m = 1000 m/s$	$c = 2652 m/s$	$c_{al} = 6000 m/s$
Acoustic Impedance	$Z_m = \rho_m c_m A$ $= 27 kg/\mathrm{s}$	$Z = \rho c A$ $= 109.8 kg/\mathrm{s}$	$Z_{alu} = \rho_{al} c_{al} A$ $= 145.8 kg/\mathrm{s}$
	$Z_{am} = -jZ_m cosec(\beta_m l_m)$	$Z_a = -jZ cosec(\beta l)$	$Z_{al} = -jZ_{alu} cosec(\beta_{al} l_{al})$
	$Z_{bm} = jZ_m tan(\beta_m l_m / 2)$	$Z_b = jZ tan(\beta l / 2)$	$Z_{bl} = jZ_{alu} tan(\beta_{al} l_{al} / 2)$

The effective bandwidth of the transducer can be changed by using different length and impedance of matching layers for fine tuning. In order to achieve a wideband transducer, we analyze the admittance seen from the acoustic ports. In Figure 4. 3 and Figure 4. 4, the normalized admittance versus normalized frequency graphs are sketched for the maximum flat admittance and the maximal bandwidth admittance. The matching layer properties of the maximum flat admittance graph are taken as $l_m \approx 0.308\lambda_m$ and $Z_m = 21.9 kg/s$. The matching layer properties of the maximum bandwidth admittance graph are $l_m \approx 0.278\lambda_m$ and $Z_m = 30\ kg/s$. We derive the maximum bandwidth response according to the two way transfer function of a transducer. We allow the variation of the two way transfer function of a reciprocal operation down to 70% of its maximum value. As a result, the ripples within Figure 4. 4 are accepted. Detailed examination of reciprocal operation can be found in Chapter 5.

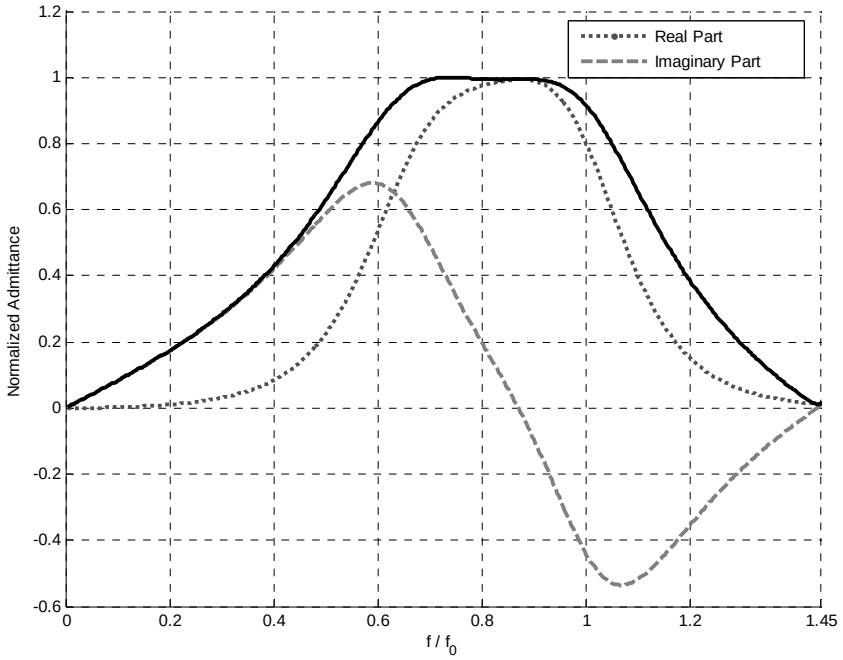

Figure 4. 3. Maximum flat admittance response of the proposed transducer.

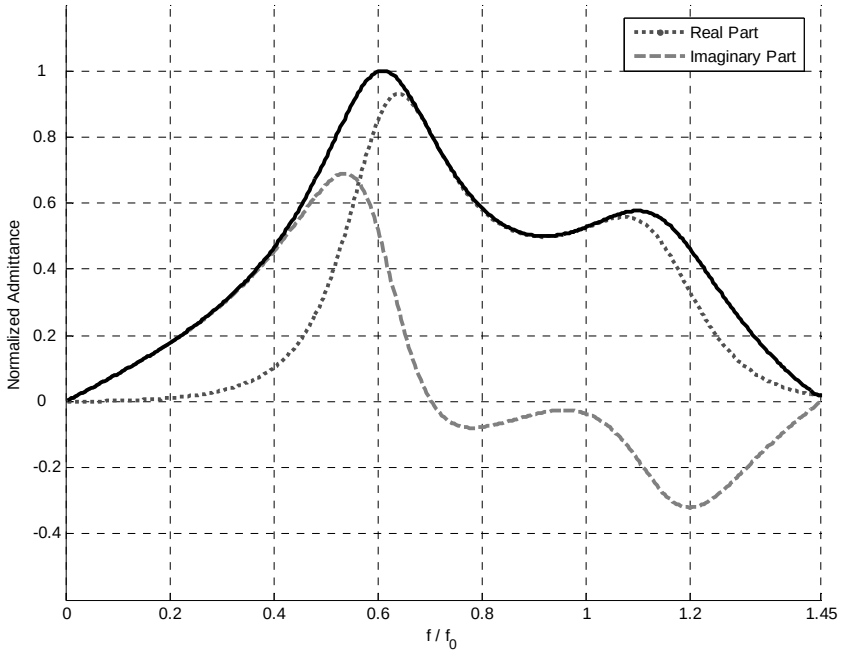

Figure 4. 4. Maximum bandwidth admittance graph of the proposed transducer.

The resonance frequency of the maximum flat response (Figure 4. 3) is less than that of the maximum bandwidth response. Both values are comparably less than the resonance frequency of a half wavelength transducer, f_0, as expected.

We excite the maximum bandwidth response transducer while the electrical port 2 is short circuited. The transfer function F_1/V_1 of the radiating port F_1, due to the unit impulse, V_1 is as depicted in Figure 4. 5. The real part of function decays fast above the frequencies, $f \approx 1.4 f_0$. The imaginary part of the transfer function is negative for $f \geq 0.6 f_0$.

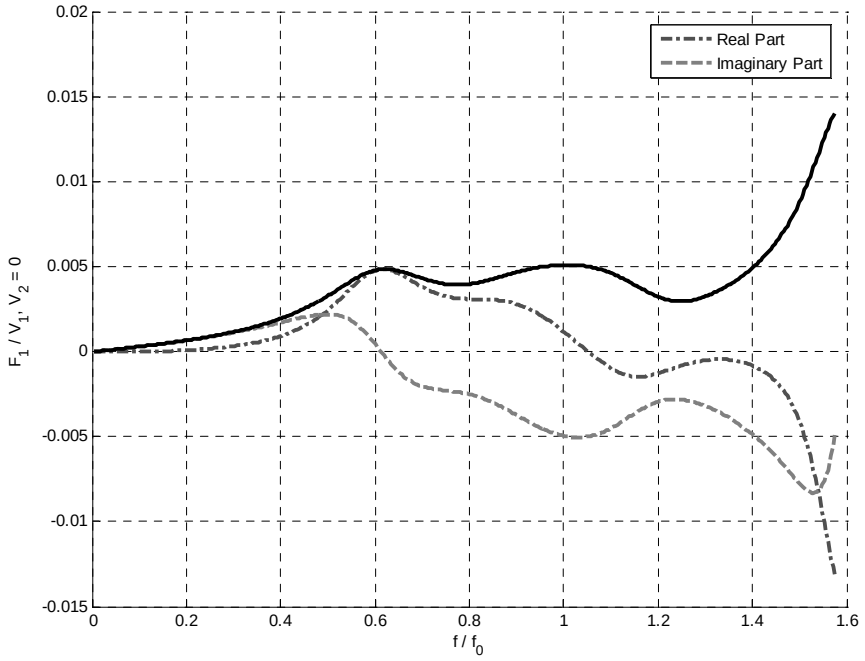

Figure 4. 5. Transfer function of maximum bandwidth transducer, F_1/V_1 when V_2 is short circuited.

The transfer function F_2/V_1 of the radiating port F_2, due to the unit impulse applied at V_1 is as depicted in Figure 4. 6. The real part of function increases fast

above frequencies, $f \approx 1.4 f_0$. The imaginary part of the transfer function is negative between $0.55 f_0 \le f \le 1.05 f_0$.

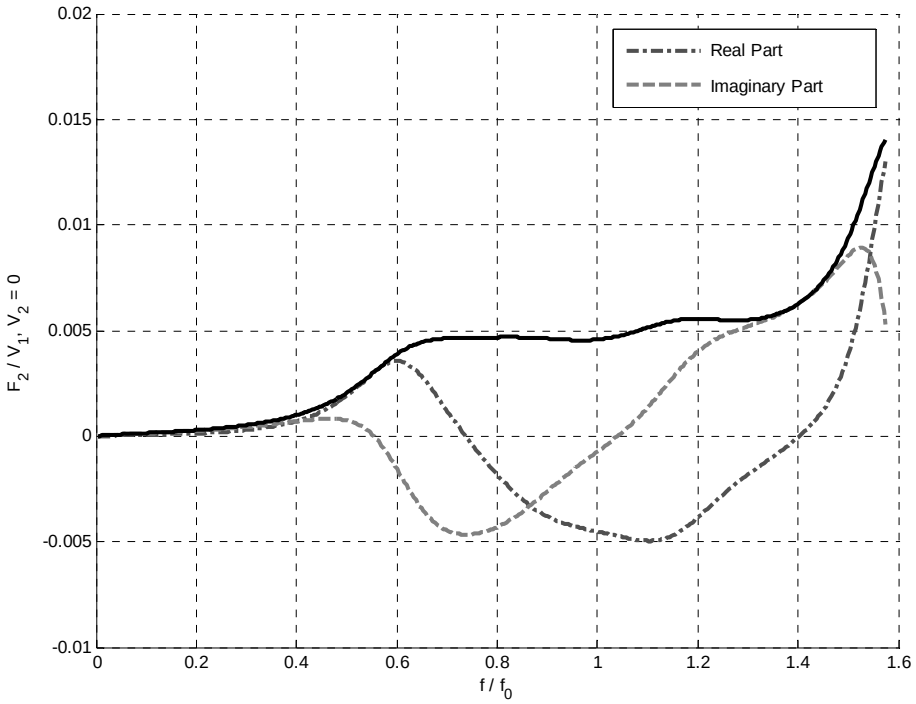

Figure 4. 6. Transfer function F_2 / V_1 when V_2 is short circuited.

We consider exciting the transducer with an impulse, when the electrical port V_1 is short circuited. Using the reciprocity theorem the transfer function F_1/V_2, of force generated on the acoustic port F_1, due to the impulse applied to V_2 is similar to the transfer function shown in Figure 4. 6. The transfer function F_2/V_2, of force generated on the acoustic port F_2, due to the impulse applied to V_2 is similar to the transfer function shown in Figure 4. 5.

$$\left.\frac{F_1}{V_1}\right|_{V_2=0} = \left.\frac{F_2}{V_2}\right|_{V_1=0}, \qquad \left.\frac{F_1}{V_2}\right|_{V_1=0} = \left.\frac{F_2}{V_1}\right|_{V_2=0}. \tag{4. 2}$$

4.2 Transmitting Mode

The proposed transducer structure is enhanced to be used for both transmit and receive modes in underwater. The transducer circuit in transmitting mode is shown in Figure 4. 7. Electrical ports V_1 and V_2 are fed by the voltage source, V_s, to maintain a parallel connection. The details of circuit parameters are given in Table II.

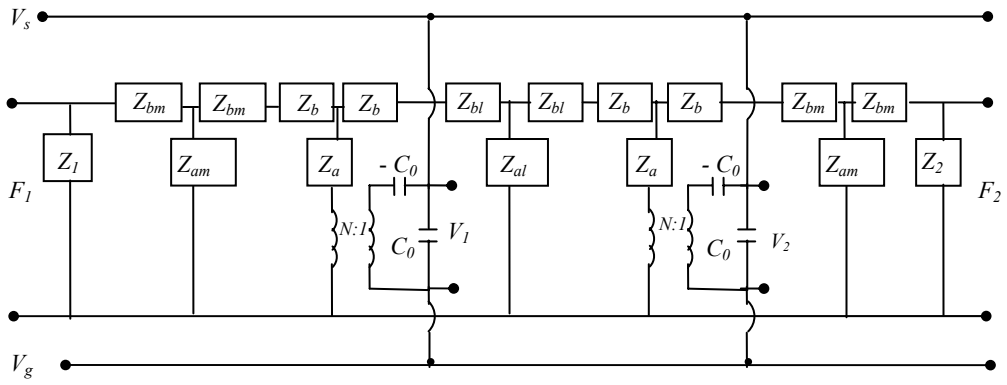

Figure 4. 7. The circuit diagram of parallel connected transmitting transducer structure.

We immerse the transducer structure in water, so that $Z_1 = Z_2 = Z_{water}$ (Figure 4. 7). We excite the electrical ports of transducer with unit impulse by applying voltage through V_s. This causes acoustic forces to be generated on the acoustic ports F_1 and F_2. Due to the symmetry of the transducer structure, equal magnitudes of forces are generated at two radiating acoustic faces ($F_1 = F_2$).

The proposed transducer structure doesn't include any tuning devices for the electrical ports V_1 and V_2, since they decrease the total output power.

Figure 4. 8 shows the transfer function F_1 / V_s of total force generated on the acoustic port F_1 due to the impulse excited on parallel connected electrical ports V_1 and V_2, versus normalized frequency. The 3 dB bandwidth of the transfer function is 87 %. Its resonance frequency is $0.856 f_0$.

The summation of transfer functions $\left.\frac{F_1}{V_1}\right|_{V_2=0}$ (Figure 4. 5) and $\left.\frac{F_1}{V_2}\right|_{V_1=0}$ (Figure 4. 6) equals the transfer function $\frac{F_1}{V_s}$ (Figure 4. 8). The resonance function is not symmetric around f_0, since the negative capacitance C_0 causes a decrease in center frequency. The transfer function F_2 / V_s is identical to the transfer function F_1 / V_s, since $V_1 = V_2 = V_s$.

The derivation of the response function F_1 / V_s is detailed in Appendix III.

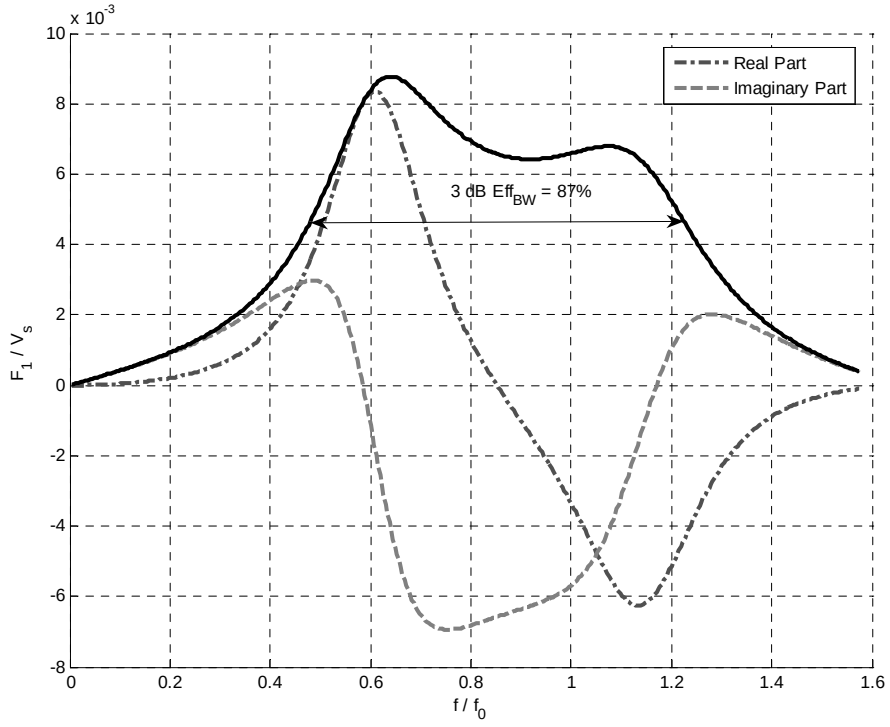

Figure 4. 8. Transfer function F_1 / V_s, where $V_1 = V_2 = V_s$.

4.3 Receiving Mode

The equivalent electrical circuit of the proposed transducer structure in receiving mode is sketched in Figure 4. 9. We connect feedback amplifiers to the electrical ports. They cancel the effect of positive capacitance due to *virtual ground*. The positive port of feedback amplifier is grounded. Its negative port is connected to the negative capacitance, - C_0. Z_{load} is inserted between the negative port and voltage outputs, V_1 and V_2. Z_{load} equals the equivalent real impedance seen before the transformer.

Acoustical waves are sensed by the acoustic ports (F_1 and F_2) in receive mode. The signals are converted to electrical pulses by the transformer.

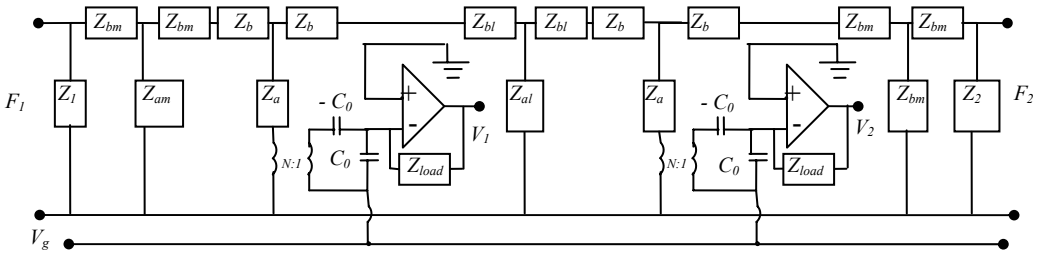

Figure 4. 9. Electrical model of receiving transducer model.

The transfer function V_1 / F_1, of voltage generated on the electrical port V_1 with respect to the unit force generated at acoustic port F_1, when F_2 is short circuited is as shown in Figure 4. 10. The 3 dB effective bandwidth of V_1 / F_1 equals 73.7%. The 3 dB bandwidth of the receiving mode transfer function is less than the 3 dB bandwidth of transmitting mode function. The function has two peaks, its real part is positive above $f \approx 1.05\ f_0$. Its imaginary part passes through zero at $f \approx 0.6\ f_0$. The magnitude of the receiving mode transfer function is greater than the magnitude of the transmitting mode transfer function (Figure 4. 8), due to the transformer ratio on the order of 0.016.

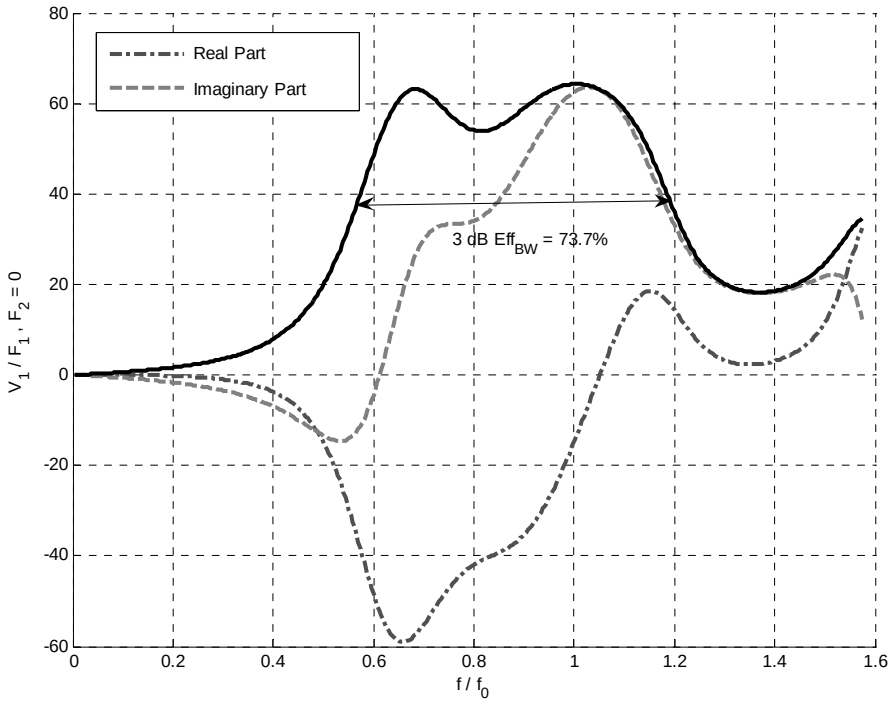

Figure 4. 10. Transfer function V_1 / F_1, when F_2 is short circuited**.**

The transfer function V_2 / F_1 of voltage generated on the electrical port V_2 with respect to a unit force generated at acoustic port F_1, when F_2 is short circuited is as shown in Figure 4. 11. The 3 dB effective bandwidth of V_2 / F_1 is 71%.

The derivation of transfer functions $\left.\frac{V_1}{F_1}\right|_{F_2=0}$ and $\left.\frac{V_2}{F_1}\right|_{F_2=0}$ are given in Appendix IV.

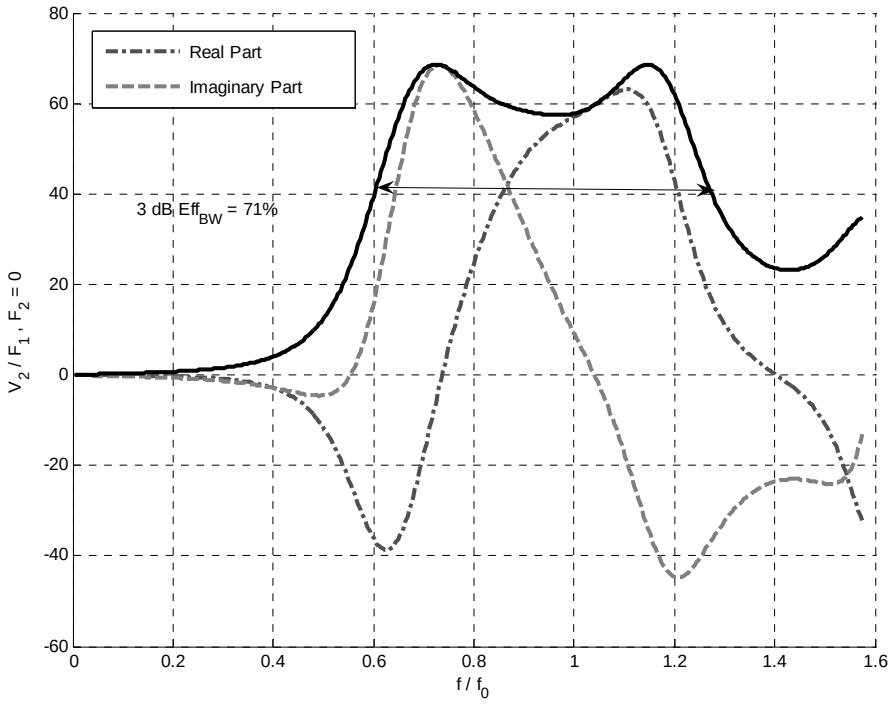

Figure 4. 11. Transfer function of V_2 / F_1 when F_2 is short circuited.

Chapter 5

Reciprocal Operation

This chapter details the reciprocal operation of the proposed transducer structure. Reciprocal operation is considered as propagation of acoustic wave from a transducer and reception at the acoustic port of another transducer, where the transducers are separated by a distance.

5.1 Boundary Conditions

The proposed transducer structure radiates equal acoustic waves into two half – spaces through its radiating ports (Figure 5. 1). The proposed transducer structure is assumed to be mounted on an infinite baffle.

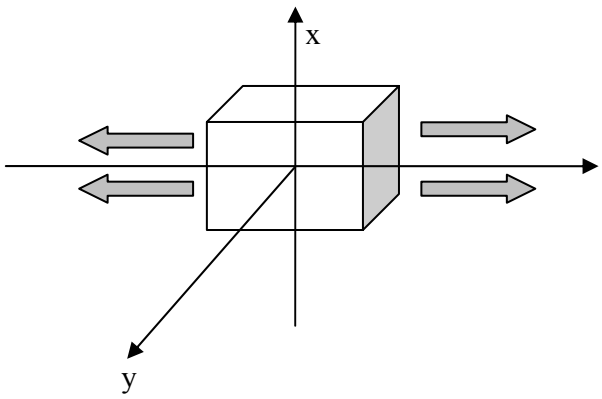

Figure 5. 1. Proposed transducer structure radiates energy into two half – spaces.

The right acoustic face is separated by a distance z_0 from the center of the transducer and radiates acoustic waves towards +z direction. The left acoustic face is separated a distance z_0 from the center of the transducer but radiates towards –z direction. Their magnitudes are the same. The radiating power from the acoustic faces result in finite potential at z = 0 plane. However, there is no net

displacement. The tangential components of the wave velocities are canceled by each other.

This assumption is consistent with the Rigid Baffle boundary definition, where there is no net displacement outside the baffle. However, there is a significant difference between the Rigid Boundary definition stated in Chapter 2 and the boundary condition of the proposed transducer structure. The former one radiates energy into one – half space and uses the image theory for basis; the latter one radiates energy into two – half spaces, and the waves propagated to the z=0 plane have 180 degrees phase difference.

5.2 Force Sensed at the Receiver Acoustic Ports

Based on the above assumption, we consider that the acoustic faces radiate energy towards the half – space that they their normal's direct as shown in Figure 5. 2.

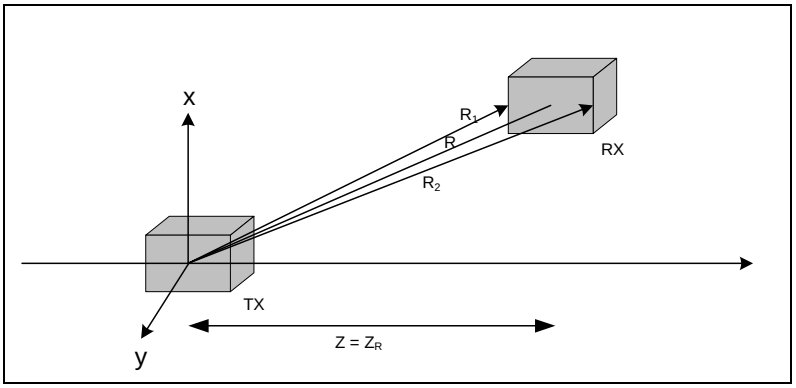

Figure 5. 2. Acoustic waves radiating from the acoustic face.
R: Distance between the radiating acoustic port and the center of the receiving port; R_1: Distance between the radiating acoustic port and the front receiving port; R_2: Distance between the radiating acoustic port and the rear receiving port.

We find the force sensed at the acoustic ports of a transducer radiated from another one - positioned at the far – field - which are separated by a distance R. For that we evaluate a solution to the boundary condition of the transducer structure in an infinite baffle, where the potential at any point ($z \geq 0$) is:

$$\phi(x,y,z) = \frac{1}{2\pi}\int_S u_0(x',y',0)\frac{e^{-jkR}}{R}ds', \tag{5. 1}$$

and

$$R = \sqrt{(z-z')^2 + (x-x')^2 + (y-y')^2}\,. \tag{5. 2}$$

Point (x',y',z') is the location of source and point (x,y,z) is the location of observation. We assume that the length of the transducer in x - direction equals $2x_0$, $2y_0$ in y - direction, besides $2z_0$ along z – direction. The displacement vector $\vec{u}_z$ is defined as below:

$$\overline{u}_Z(x,y,z) = \hat{a}_z u_0\,. \tag{5. 3}$$

Using Eq. (5.1), the potential at point *(x,y,z)* is simplified to:

$$\phi = -\frac{u_0}{2\pi}\int_{S_1}\frac{e^{-jkR}e^{\frac{jk(x'x+y'y)}{R}}}{R}e^{\frac{jkz_0 z}{R}}dx'dy'\,. \tag{5. 4}$$

Since force at the rear acoustic port equals:

$$F(z-z_0) = \int_{-x_0}^{x_0}\int_{-y_0}^{y_0} p\,dxdy\,, \tag{5. 5}$$

and

$$p = w^2\rho\phi\,, \tag{5. 6}$$

the force generated at the front acoustic port of the receiver is:

$$F(z-z_0) = -\frac{kF_0}{j2\pi} A \frac{e^{-jkR}}{R} \sin c(\frac{kx_0 x}{R}) \sin c(\frac{ky_0 y}{R}) e^{\frac{jkz_0 z}{R}} e^{jkz_0 \cos\theta \cos\varphi} \sin c(kx_0 \sin\theta) \sin c(ky_0 \sin\varphi \cos\theta). \quad (5.7)$$

(φ, θ) are the rotation angles of the receiver with respect to the transmitter along z-y plane and around y - direction (Figure 5. 3).

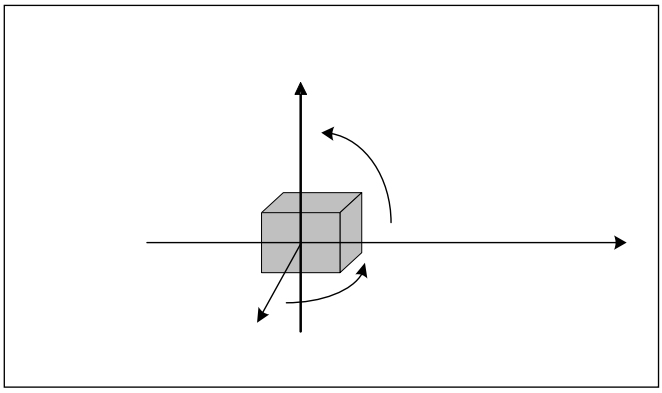

Figure 5. 3. Rotation of receiving transducer around its axes.

In a similar way, we derive the force generated at the rear acoustic port of the receiver:

$$F(z+z_0) = -\frac{kF_0}{j2\pi} A \frac{e^{-jkR}}{R} \sin c(\frac{kx_0 x}{R}) \sin c(\frac{ky_0 y}{R}) e^{\frac{jkz_0 z}{R}} e^{-jkz_0 \cos\theta \cos\varphi} \sin c(kx_0 \sin\theta) \sin c(ky_0 \sin\varphi \cos\theta). \quad (5.8)$$

Detailed derivation of force generated on acoustic faces is given in Appendix V.

We examine the behavior of acoustic waves radiated from the transmitter which are sensed by the acoustic ports of a receiver. The source transducer is fed with unit impulse, and acoustic waves are propagated though the water. As a result electrical voltage is formed on both electrical ports of the receiving transducer at the observation point. The transducer properties are as described in Chapter 4. The source and observing transducers are oriented on the same x – y plane, (φ,θ) = (0,0). The distance between the centers of transducers, Z_R is kept 10 meters.

The transfer function V_1 / V_s, of voltage generated on the front electrical port V_1 with respect to the unit impulse generated at the electrical ports of transmitting transducer, V_s when the rear acoustic port, F_2 is short circuited, is as shown in Figure 5. 4. The real part of the response function crosses the zero value three times. It is negative for $0.75 f_0 \le f \le 1.22 f_0$. The function employs two peaks. The 6 dB effective bandwidth of the transfer function is 77 %.

The transfer function V_1 / V_s, of voltage generated on the front electrical port V_1 with respect to the unit impulse generated at the electrical ports of transmitting transducer, V_s when the front acoustic port, F_1 is short circuited, is as shown in Figure 5. 5. The real part of the response function crosses the zero value two times. It is negative between $0.95 f_0 \le f \le 1.48 f_0$. The imaginary part is positive for frequencies less than $1.3 f_0$. The transfer function employs two peaks. Its 6 dB effective bandwidth equals 73.4%.

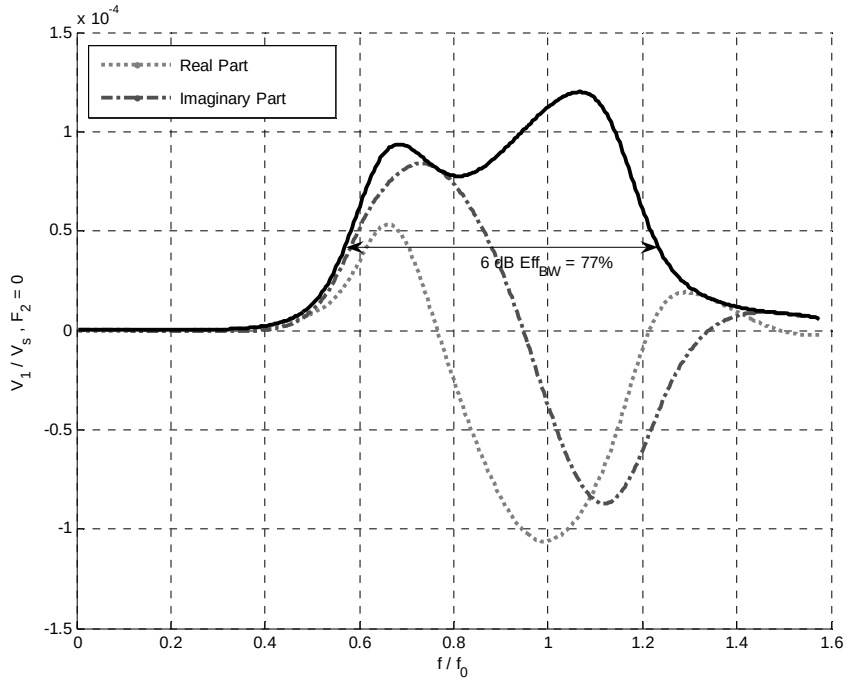

Figure 5. 4. Transfer function V_1 / V_s where $F_2 = 0$.

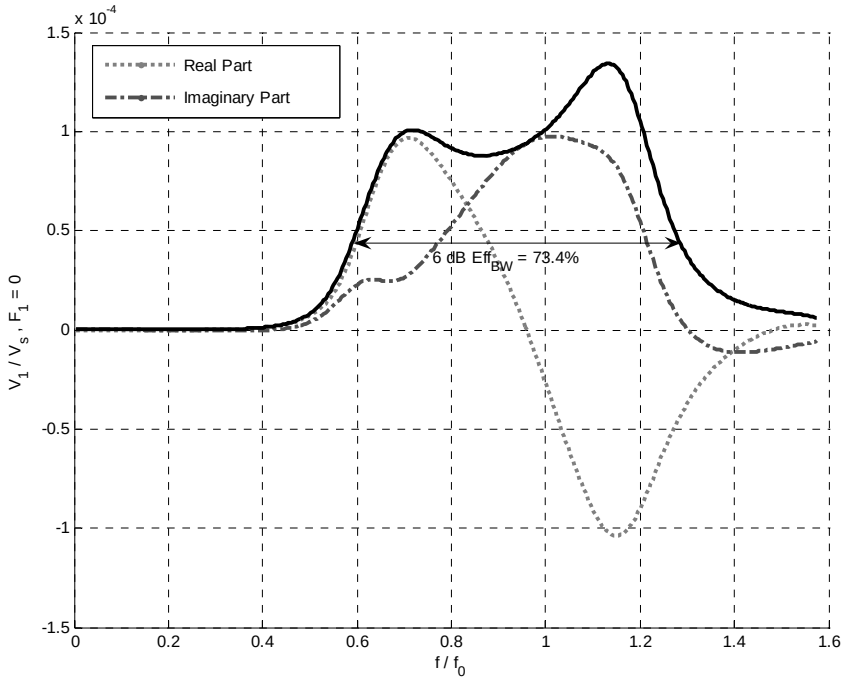

Figure 5. 5. Transfer function V_1 / V_s where $F_1 = 0$.

The transfer function V_2 / V_s, of voltage generated on the rear electrical port V_2 with respect to the unit impulse generated at the electrical ports of transmitting transducer, V_s when the front acoustic port, F_1 is short circuited, is as depicted in Figure 5. 6. The real and imaginary parts of the function crosses zero three times. The 6 dB effective bandwidth of the response function is 75.5%.

The transfer function V_2 / V_s, of voltage generated on the rear electrical port V_2 with respect to the unit impulse generated at the electrical ports of transmitting transducer, V_s when the rear acoustic port, F_2 is short circuited, is as depicted in Figure 5. 7. The real and imaginary parts of the function crosses zero four times. The 6 dB effective bandwidth of the transfer function is 74.5%.

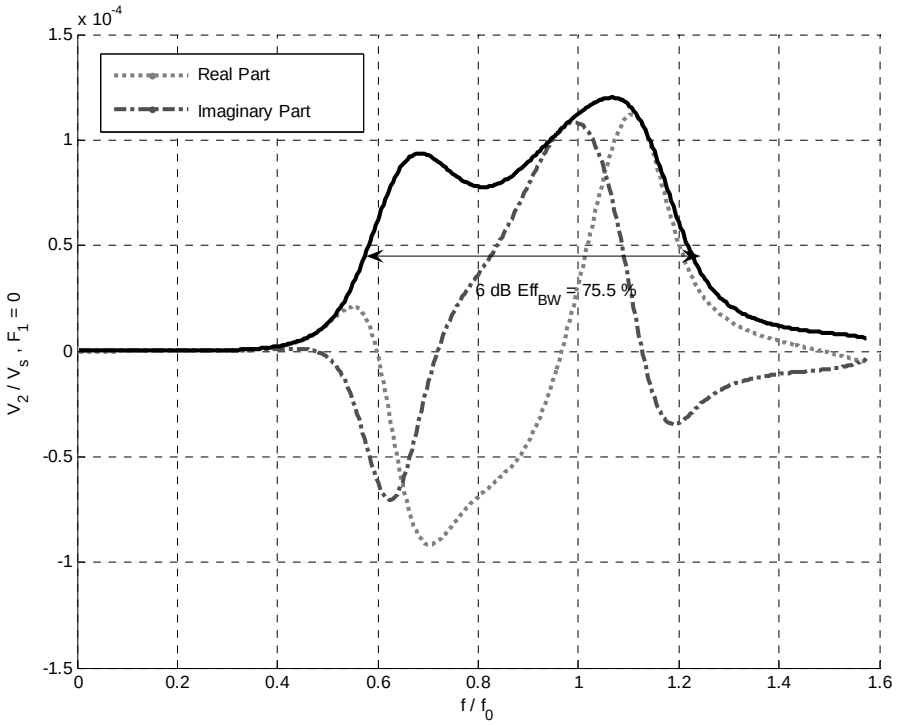

Figure 5. 6. Transfer function V_2 / V_s where $F_1 = 0$.

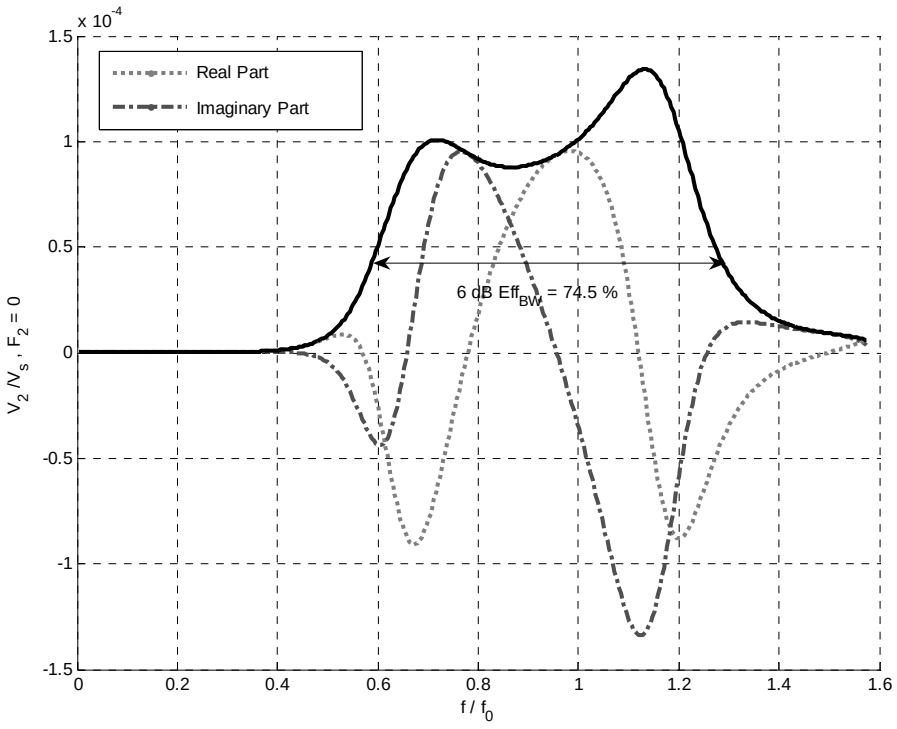

Figure 5. 7. Transfer function V_2 / V_s where $F_2 = 0$.

Figure 5. 8 and Figure 5. 9 show the overall voltage transfer functions that are determined at the electrical ports V_1 and V_2 of the receiving transducer when a unit impulse is generated at the electrical ports of the transmitting transducer. The absolute values of two transfer functions are the same. They have two peaks at frequencies $0.68f_0$ and $1.1f_0$. The magnitude of response function is maximum at $f = 1.1\, f_0$. Their 6 dB effective bandwidth equals 78%.

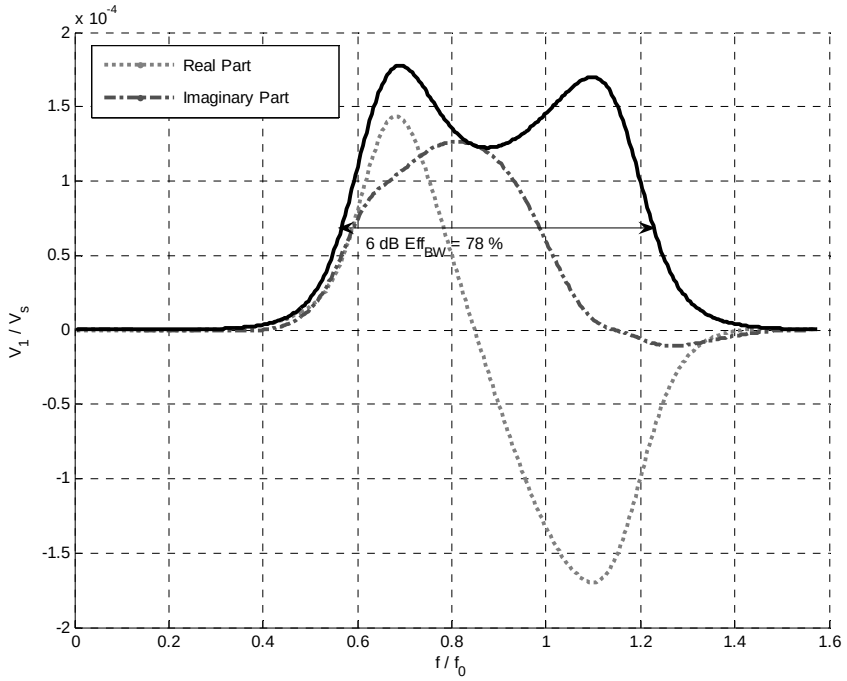

Figure 5. 8. Overall transfer function V_1 / V_s.

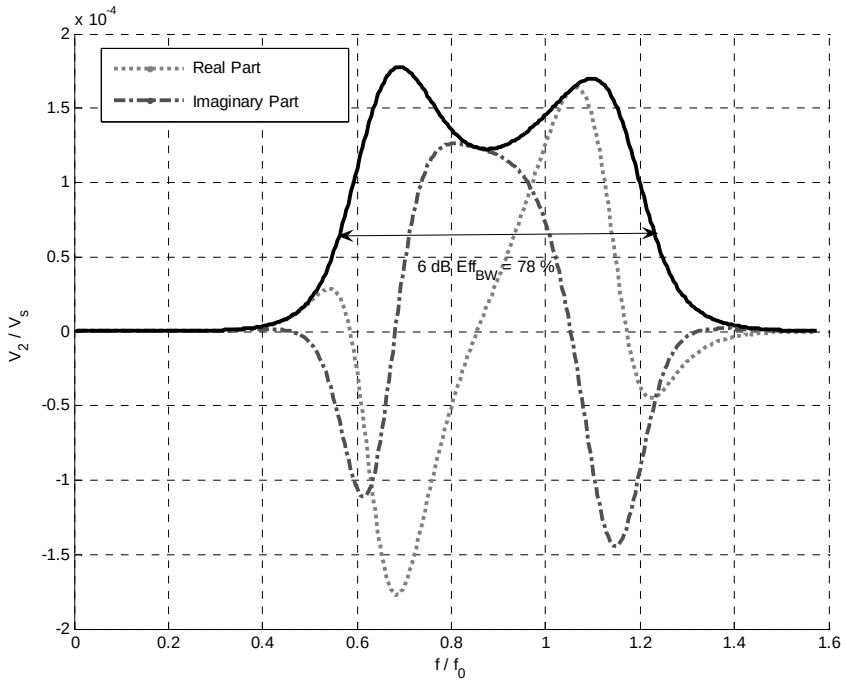

Figure 5. 9. Overall transfer function V_2 / V_s.

There is a constant phase difference between the transfer functions V_1 / V_s and V_2 / V_s. Acoustic signals reach the rear receiving face 5.9 μsec after they reach the front receiving face, which can be shown by:

$$\frac{V_1}{V_s} = \frac{V_2}{V_s} e^{-jw\Delta t}, \tag{5. 9}$$

where Δt equals 5.9 μsec.

The electrical signal is sensed at the front electrical port earlier than the rear one, because it takes more time for an acoustic wave to propagate the length of the transducer and reach the rear acoustic port. The phase difference between the received functions is used to delay the electrical signal sensed at the front electrical port for constructively addition. We delay V_1 / V_s and sum with V_2 / V_s. The delayed and summed overall transfer function $\frac{V_2}{V_s} + \frac{V_1}{V_s} e^{jw\Delta t}$ is as shown in Figure 5. 10. By this way, the signals generated at the electrical ports are effectively used.

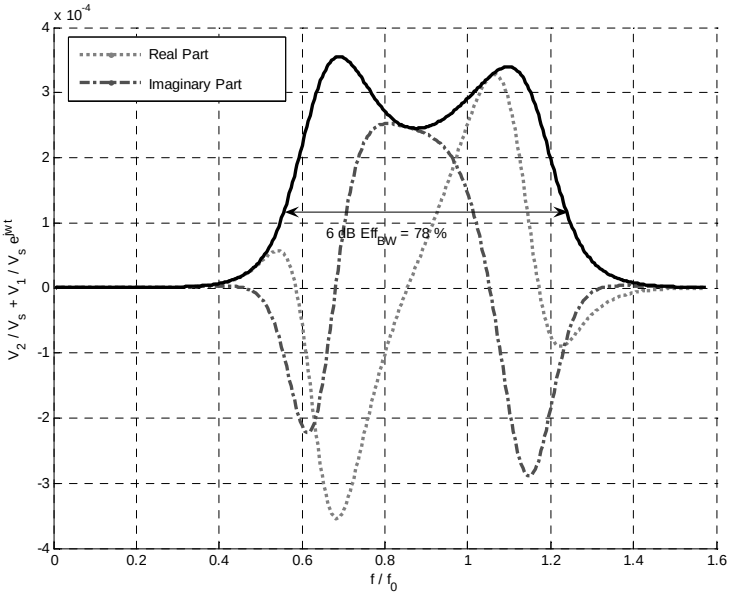

Figure 5. 10. Delayed and summed transfer function, $\frac{V_2}{V_s} + \frac{V_1}{V_s} e^{jw\Delta t}$.

Chapter 6

Results

In this chapter, we analyze several reciprocal operation characteristics of the proposed transducer structure.

6.1 Changing the Distance within a Wavelength

We change the distance between receiving and transmitting transducers and examine the response of the system that is aligned on the z – axis. We increase the distance between two transducers with λ / 4 long multiples from 10 meters (Figure 5. 10) up to 10 meters and a wavelength long. The transfer functions are as sketched in Figure 6. 1. The magnitude of the transfer functions are not affected from changing the distance within a wavelength. Each has its 6 dB effective bandwidth equal to 78 %. On the other hand, the magnitudes of real and imaginary parts of transfer functions are changed as the separation of receiving and transmitting transducers are changed.

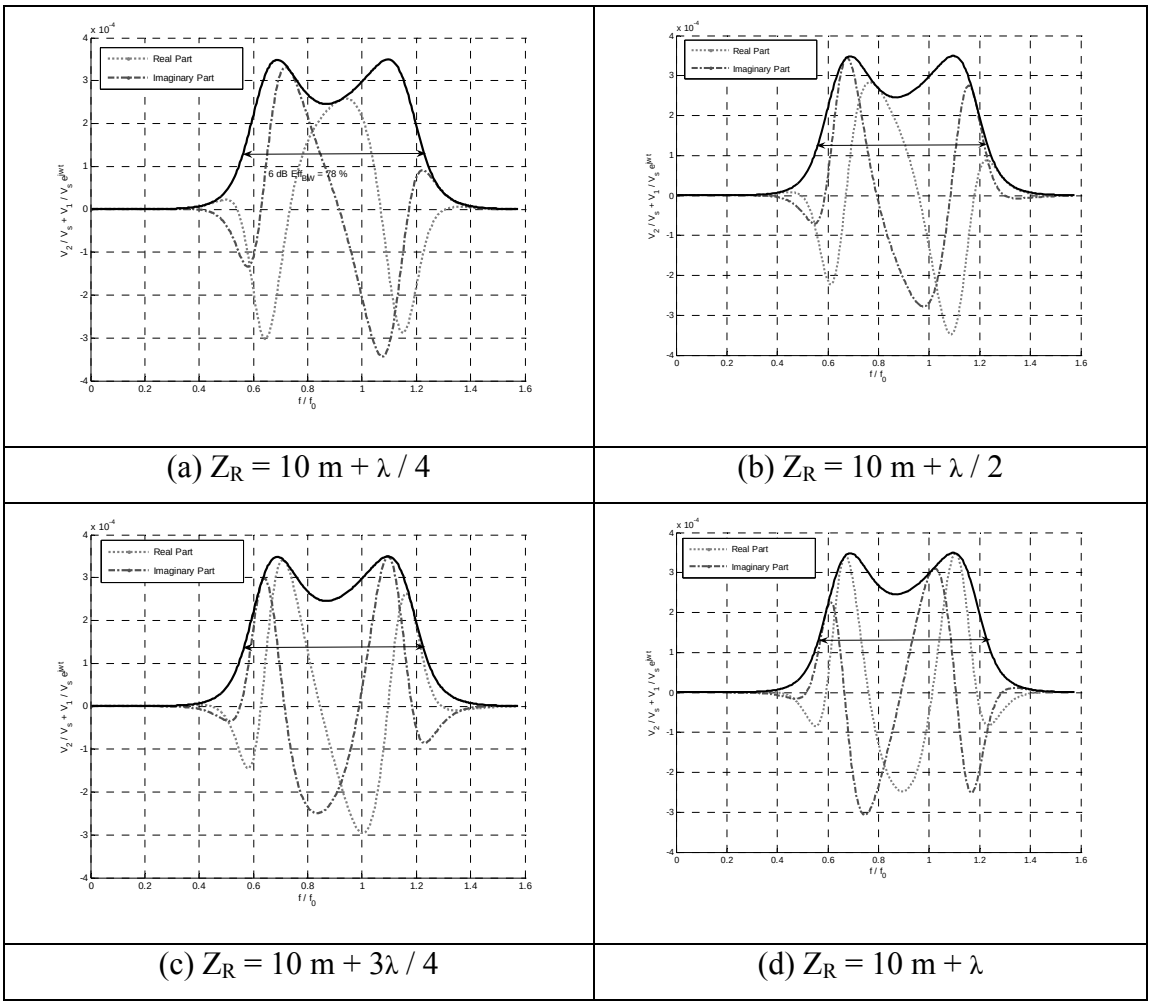

(a) Z_R = 10 m + λ / 4 | (b) Z_R = 10 m + λ / 2

(c) Z_R = 10 m + 3λ / 4 | (d) Z_R = 10 m + λ

Figure 6. 1. Transfer function $\frac{V_2}{V_s} + \frac{V_1}{V_s} e^{jw\Delta t}$ where distance between transducers is:

(a) Z_R = 10 m + λ / 4, b) Z_R = 10 m + λ / 2, (c) Z_R = 10 m + 3λ / 4,

(d) Z_R = 10 + λ m.

6.2 Rotating the Receiving Transducer

We examine the response of the reciprocal system based on the alignment of the receiving transducer. We derive the transfer function $\frac{V_2}{V_s} + \frac{V_1}{V_s} e^{jw\Delta t}$ with respect to normalized frequency range for different θ angles; where θ is the angle between the center of the receiving transducer and $z=z_R$ plane. The separation between the

mid - points of the two transducers, z_R is kept at 10 meters. The alignment of the transmitting transducer is not changed as shown in Figure 6. 2.

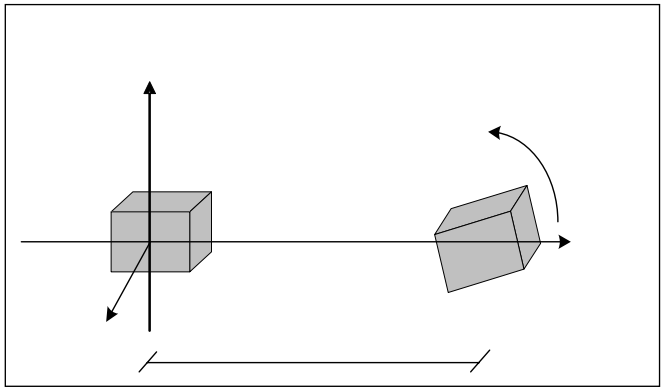

Figure 6. 2. Alignment of receiver with respect to transmitting transducer.

The resultant delayed and constructively added transfer functions are as shown in Figure 6. 3. The 6 dB bandwidth of the transfer function when $\theta = 2^o$ equals 77 % (Figure 6. 3a). The transfer function is similar to the one where $\theta = 0^o$ (Figure 5. 10), with the exception of a slightly lower magnitude. The 6 dB bandwidth when θ equals 5^o is 75.2 % (Figure 6. 3b). The resultant function employs two peaks. The peak at the higher frequency $f = 1.1f_0$ has lower magnitude compared to the one at $f = 0.68f_0$. The 6 dB bandwidth of the transfer function when $\theta = 15^o$, equals 39 % (Figure 6. 3c). The peak at $f = 1.1f_0$ is nearly disappeared and the maximum value of the transfer function is fifty percentage compared to the maximum value of the response function where θ equals 0^o. When $\theta = 22^o$ (Figure 6. 3d), the 6 dB bandwidth of the transfer function equals 34.3 %. There is a notch at $f = 1.1f_0$ where a peak exists when $\theta = 0^o$. The transfer function of $\theta = 27^o$ case employs two peaks at $f = 0.62f_0$ and $f = 1.15f_0$ besides a notch at $f = 1.1f_0$ (Figure 6. 3e). For $\theta = 90^o$, there are three peaks and two notches. However, the maximum absolute value of the response function is negligible when compared to that of the $\theta = 0^o$, which is 5% of its magnitude (Figure 6. 3f).

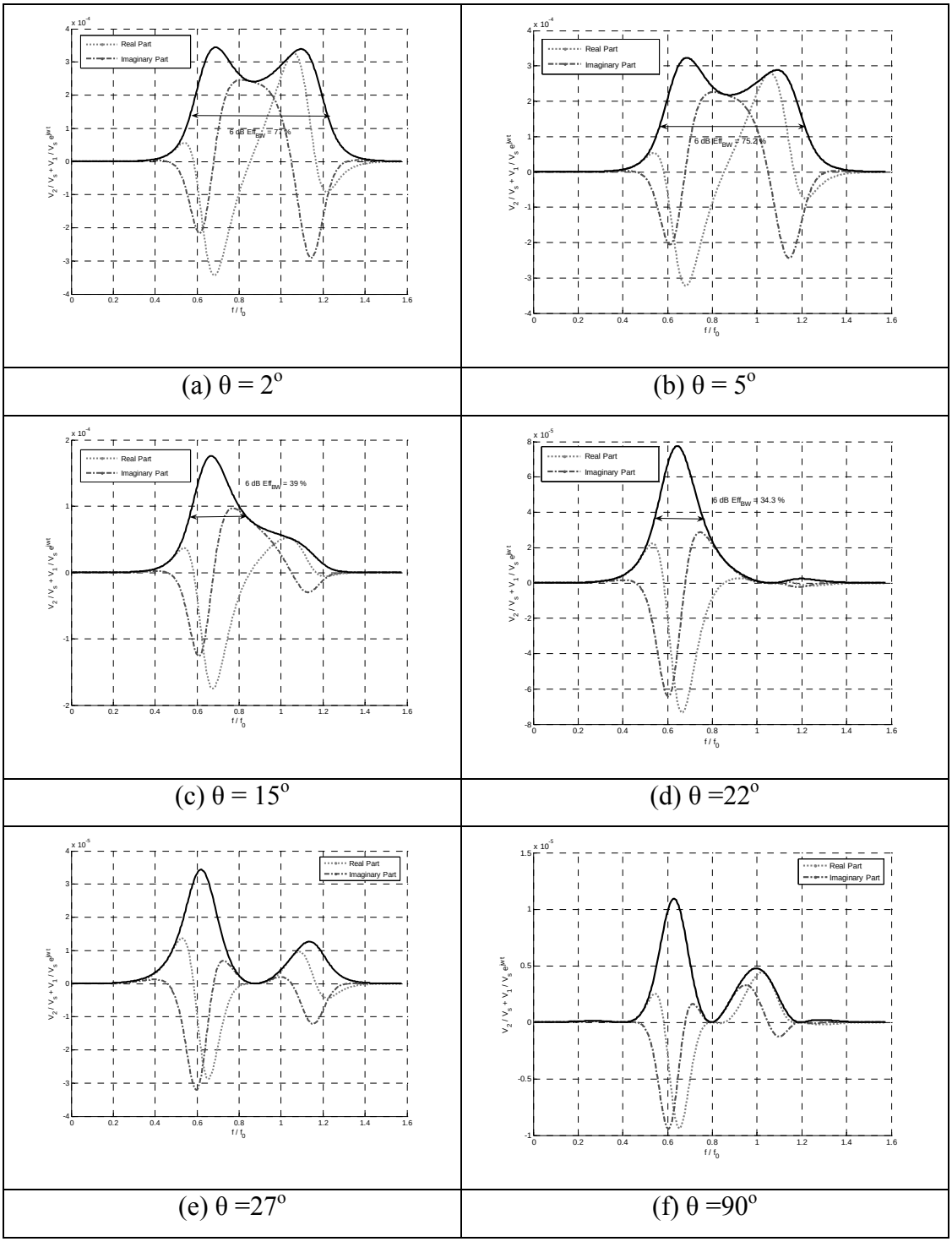

(a) θ = 2°

(b) θ = 5°

(c) θ = 15°

(d) θ =22°

(e) θ =27°

(f) θ =90°

Figure 6. 3. Transfer functions where a) θ = 2°, b) θ = 5°, c) θ = 15°, d) θ = 22°, e) θ = 27° and f) θ = 90°.

The transfer function $\frac{V_2}{V_s} + \frac{V_1}{V_s} e^{jw\Delta t}$ results the same when center point of the receiver is aligned at $z = z_R$ and the receiving transducer is rotated to φ = 2°, 5 °, 15 °, 22 °, 27 ° and 90 °, where φ is the angle between the acoustic face of the receiver and $z = z_R$ plane.

6.3 Fixed Frequency Response

We examine the transfer response of the system, shown in Figure 6. 2, based on rotation of the receiver at a fixed frequency. The receiver is rotated around its center perpendicular to the y – axis ($0 \leq \theta \leq 2\pi$). Figure 6. 4 shows the polar response functions at $f=0.675f_0$, $0.9\ f_0$ and $1.125\ f_0$. The magnitude of the response equals half of its maximum for $f = 0.675\ f_0$ when θ equals 30°. When f equals $0.9\ f_0$, the 6 dB beamwidth of the polar pattern is 22°. The 6 dB beamwidth of the radiation pattern for $f = 1.125\ f_0$ equals 17.5°.

Figure 6. 5 shows the 6 dB effective beamwidth of the reciprocal system with respect to normalized frequency. The beamwidth decreases as the frequency increases. It is concluded that as the operational frequency increases, the directivity of the transducer increases and hence, the effective beamwidth decreases.

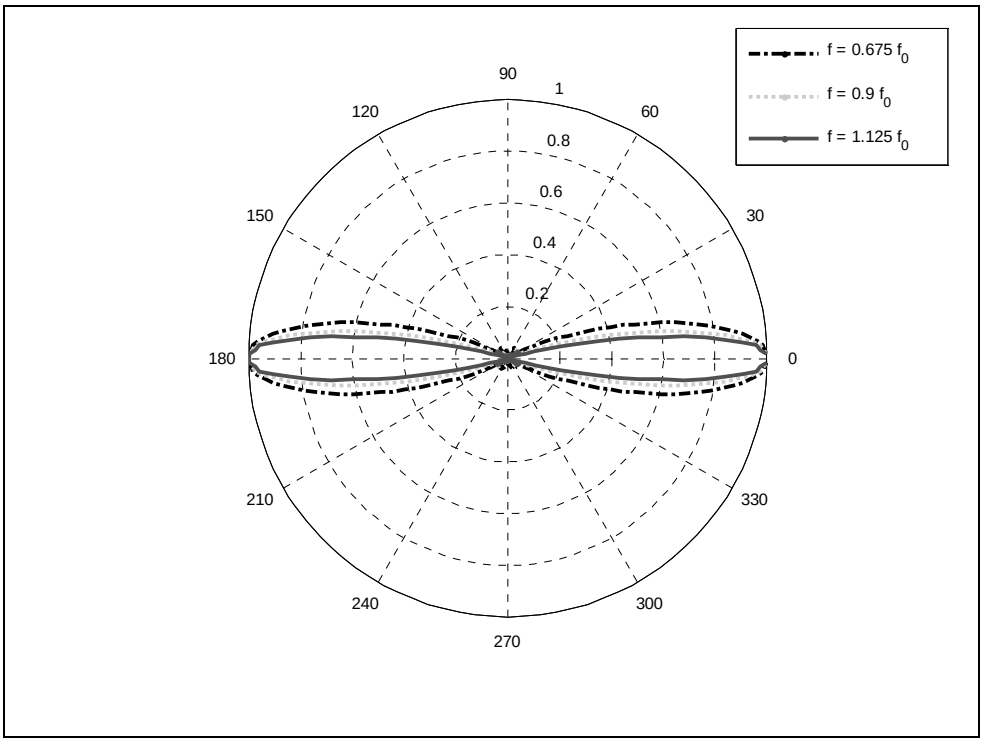

Figure 6. 4. Rotating the receiver around y - axis at fixed frequencies:
a) $f = 0.675\, f_0$, b) $f = 0.9\, f_0$, c) $f = 1.125\, f_0$.

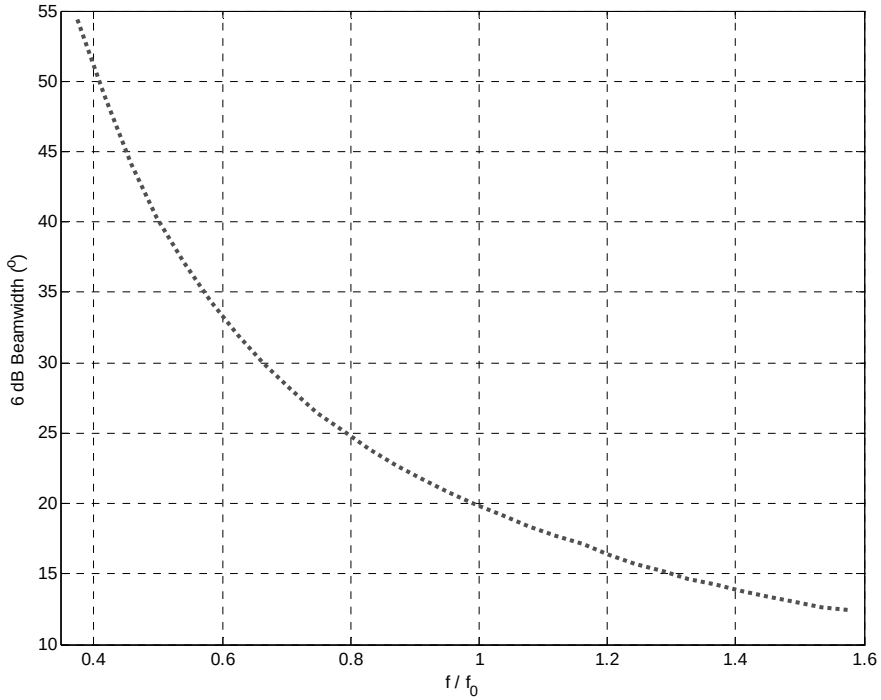

Figure 6. 5. Effective beamwidth versus normalized frequency.

6.3 Acoustic Face Dimensions

We examine the response of the transducer structures with different square shaped acoustic face areas, A. We compare the transfer functions $\frac{F_1}{V_s}$, the force generated at the acoustic ports of the transmitting transducer to a unit impulse generated at the parallel connected electrical ports with surface areas, $A = 9*10^{-6} m^2$ and $A = 4*10^{-6} m^2$. The absolute values of transfer functions are as sketched in Figure 6. 6. The 3 dB effective bandwidths of transfer functions are equal to each other, 87%. However, the magnitude of the transfer function for $A = 4*10^{-6} m^2$ is 4 / 9 times less than the magnitude of the transfer function for $A = 9*10^{-6} m^2$.

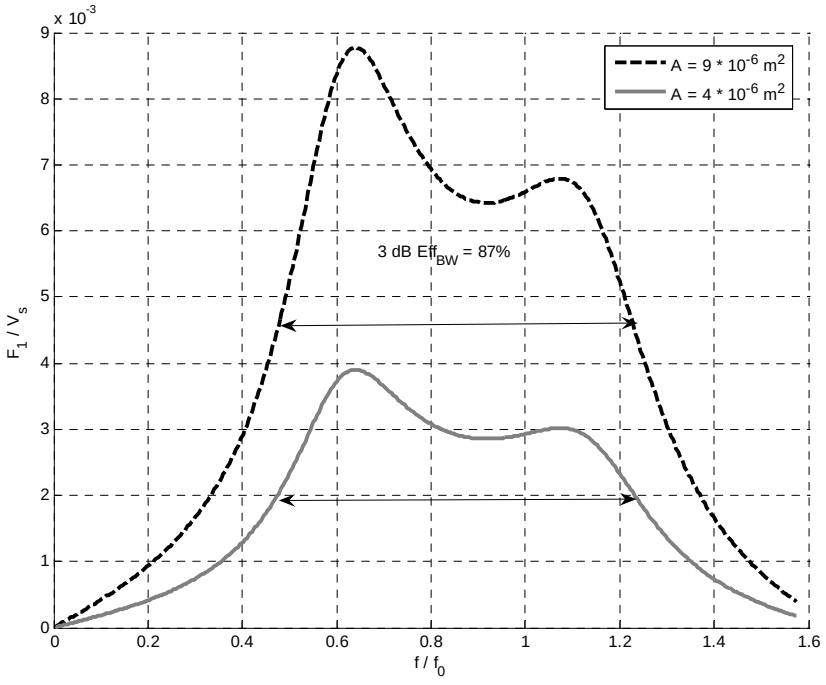

Figure 6. 6. Transfer functions $\frac{F_1}{V_s}$, for $A = 4*10^{-6} m^2$ and $A = 9*10^{-6} m^2$.

We compare the response functions $\frac{V_1}{V_s}$, of reciprocal transducers where $A = 9*10^{-6} m^2$ and $A = 4*10^{-6} m^2$. For both cases, we rotate the receiving transducer around its center, perpendicular to the y – axis ($0 \leq \theta \leq 2\pi$), at a fixed frequency $f=0.675f_0$. The 6 dB beamwidth of the polar function for $A = 9*10^{-6} m^2$ equals 30º. It is 46º when $A = 4*10^{-6} m^2$.

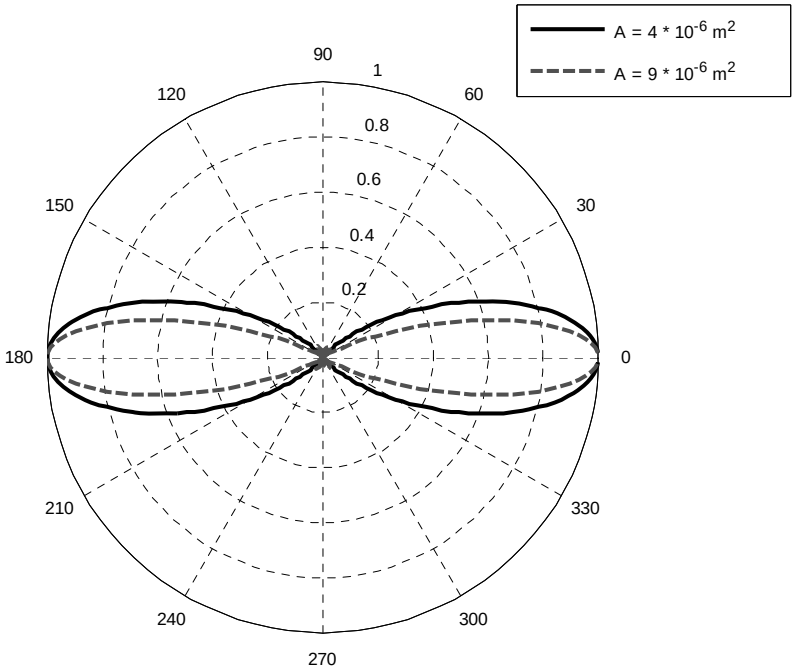

.Figure 6. 7. Polar plots for $A = 4*10^{-6} m^2$ and $A = 9*10^{-6} m^2$ when the receiving transducer is rotated around its center ($0 \leq \theta \leq 2\pi$), at a fixed frequency, $f=0.675f_0$.

Chapter 7

Conclusions

In this thesis, we discussed how to design a wideband transducer operating in underwater at high frequencies.

We found analytically that a quarter – wavelength composite piezoelectric layer connected to another one using a very thin aluminium layer and matched to water at both sides can be assumed as a structure in an infinite baffle. As a result, the transducer propagates acoustic waves through its acoustic ports, and introduces propagation to two half – spaces.

It is seen that the transducer model introduced in this thesis has many advantages over the air – backed transducers which limit the propagating space of acoustic waves into one half – space in water.

We matched the transducer structure to water for a maximal bandwidth transfer function. The amplitudes over the operational frequency range are let to vary down to 3 dB of the reciprocal transfer function results. Hence, the effective bandwidth of the transducer is increased.

Conventionally, the transducer is modeled for receiving and transmitting purposes. The two electrical ports of the transducer are connected parallel to each

other. Feedback amplifiers are connected to two acoustic ports of the receiving transducer.

To test the designs, we performed simulations. The simulations showed that there exists a constant phase difference between the signals formed at the electrical ports of the receiver when an acoustic wave is radiated from the transmitter. We added the two electrical signals constructively in order to increase the sensitivity.

We discussed the effective bandwidth of the transducer for different placements of the receiver with respect to the transmitter placed in underwater. The effective bandwidth of the transfer functions are not affected from changing the distance between receiver and transmitter when the distance is changed within a wavelength of the transducer.

It is seen that the effective beamwidth of the proposed transducer is narrow. This is due to the length of the ceramic layer which is long compared to the wavelength of sound wave in water. In order to improve the beamwidth, the surface area of the transducer can be decreased. The simulation results showed that the beamwidth increases and the magnitude of the received acoustic force decreases when the surface area is decreased. Decreasing surface area, however, also decreases the real part of the impedance. Hence, there will be poor acoustic coupling.

In the light of analytical and numerical findings, we conclude that the wideband bi – directional transducer modeling can have a good potential in spread spectrum techniques and it can be utilized effectively in underwater voice and data transmissions.

A possible future research could be to use other ceramic materials which have lower sound velocity, instead of a PZT-5A and stycast composite in order to

decrease the length of the composite piezoelectric layer and increase the beamwidth.

Using three orthogonally placed transducer structures for receiving and transmitting modes can be investigated. Such a structure may improve beamwidth. Further research is necessary to fully exploit the potential provided by two separate electrical ports. Better active and / or passive termination of the electrical ports will provide a control over both sensitivity and directional response.

BIBLIOGRAPHY

[1] Milica Stojanovic, "Recent advances in high – speed underwater acoustic communications", *IEEE Journal of Oceanic Engineering*, vol. 21, no.2, pp. 125-136, April 1996.

[2] Azizul H. Quazi and William L. Konrad, "Underwater acoustic communications", *IEEE Communications Magazine*,vol. 20, pp. 24 – 30, 1982.

[3] Bryan Woodward, "Digital underwater acoustic voice communications", *IEEE Journal of Oceanic Engineering,* vol. 21, no. 2, 1996.

[4] Milica Stojanovic. Underwater Acoustic Communication. http://www.mit.edu/~millitsa/resources/pdfs/ency.pdf.

[5] Radio History, http://earlyradiohistory.us

[6] Robert J. Urick *Principles of Underwater Sound.* McGraw-Hill Book Company, 1983.

[7] M. Stojanovic, J. Catipovic and J. G. Proakis, "Adaptive multichannel combining and equalization for underwater acoustic communications", *The Journal of Acoustic Society of America,* vol. 94, pp. 1621 – 1631, 1994.

[8] Ethem M. Sozer, Milica Stojanovic, J. G. Proakis, "Underwater acoustic networks", IEEE Journal of Oceanic Engineering, vol. 25, no.1, pp.72 – 83, January 2000.

[9] R. Coates and P. Willison, "Underwater acoustic communications: A review and bibliography", Proc. Inst. Acoust., Dec, 1987.

[10] Kim C. Benjamin and Sheridan Petrie, "A new navy calibration standard transducer using 1-3 piezocomposite", *Oceans 2000 MTS/IEEE Conference and Exhibition*, vol. 2, pp. 1299 – 1304, 2000.

[11] Piezocomposite Materials, www.morgan-electroceramics.com.

[12] Piezocomposite Transducer Design, http://www.matsysinc.com/products/ sonar_transducers/docs/ Piezocomposite_Transducer_Design.pdf.

[13] W. A. Smith, "Modeling 1 – 3 Composite Piezoelectrics: Thickness Mode Oscillations," *IEEE Trans. Ultrason. Ferroelec. Freq. Contr.*, vol. 38, pp. 40 – 46, 1991.

[14] Rodney F. W. Coates, "The design of transducers and arrays for underwater data transmission", *IEEE Journal of Oceanic Engineering*, vol. 16, no. 1, 1991.

[15] Gordon S. Kino, *Acoustic Waves: Devices, Imaging and Analog Signal Processing*. Prentice Hall, 1987.

[16] W. A. Smith, "The Role of Piezocomposites in Ultrasonic Transducers", *1989 IEEE Ultrason. Symp.*, pp. 755 – 766, 1989.

[17] G. Kossof, "The effects of backing and matching on the performance of piezoelectric ceramic transducers", *IEEE Trans. Sonics Ultrason.*, vol. SU-13, pp. 20 – 30, 1996.

[18] E. A. Neppiras, "The pre-stressed piezoelectric sandwich transducer", *Proc. Ultrason. Int. 1973 Conf.,* pp. 296 – 302, 1973.

[19] D. Stansfield, *Underwater Electroacoustic Transducers*. Bath, UK: Bath Univ. Press, 1990.

[20] W. A. Smith, "Modeling 1 – 3 composite piezoelectrics: Hydrostatic Response", *IEEE Trans. Ultrason. Ferroelec. Freq. Contr.*, vol. 40, pp. 41 – 49, 1993.

Appendix I

Green's Function

The spherically symmetric solution of the wave equation implies that the potential at the point *x, y, z* of a longitudinal wave due to a source at a point x', y', z' can be written in the form:

$$G = \frac{Ae^{-jkR}}{R}, \tag{I. 1}$$

where

$$R = \sqrt{(x-x')^2 + (y-y')^2 + (z-z')^2}\ . \tag{I. 2}$$

Eq (IV.1) is a solution of the wave equation for a source point at x', y', z' with

$$\nabla^2 G + k^2 G = \delta(x-x', y-y', z-z'), \tag{I. 3}$$

where x', y', z' are the independent variables, so all differentiations are with respect to the variables x', y', z'. The function $\delta(x-x', y-y', z-z')$ is the three dimensional Dirac delta function, which satisfies the equation

$$\int_{-\infty}^{\infty}\int_{-\infty}^{\infty}\int_{-\infty}^{\infty} \delta(x-x', y-y', z-z')dx'dy'dz' = 1, \tag{I. 4}$$

with $\delta(x-x', y-y', z-z') \to \infty$ as $R \to 0$.

Eq (I.1) satisfies the boundary condition at infinity and corresponds to a wave propagating outward from the point *x, y, z*. The function *G* is called the *free – space Green's function*. To find the constant *A*, we integrate Eq. (I. 3) over a small sphere of radius *a*, enclosing the point *x, y, z*. Thus

$$\int_{a\to 0} (\nabla^2 G + k^2 G) dV = 1. \tag{I. 5}$$

Using Gauss's theorem, it follows that the first term in the integral becomes

$$\int_{s_a} \nabla G \cdot \mathrm{n}\, ds = -4\pi A, \tag{I. 6}$$

where s_a is the surface of the sphere. The second term in the integrand becomes

$$k^2 \int_{a\to 0} G dV = 4\pi k^2 A \int_{a\to 0} \frac{1}{R} R^2 dR = 0. \tag{I. 7}$$

It is apparent, therefore that as $a \to 0$, $A \to -1/4\pi$. Thus the free – space Green's function is:

$$G = \frac{-e^{-jkR}}{4\pi R}. \tag{I. 8}$$

APPENDIX II

Transducer Matrix

The external force applied to the piezoelectric material at the surface of the resonator is:

$$F = AT, \tag{II. 1}$$

where A is the surface area of the transducer and T is the internal stress.

The direction of the particle velocity is inwards to the piezoelectric material. We can derive the boundary conditions at the acoustic ports such as:

$$\begin{aligned} F_1 &= AT(\frac{-l}{2}), \\ F_2 &= AT(\frac{l}{2}), \\ v_1 &= v(\frac{-l}{2}), \\ v_2 &= -v(\frac{l}{2}). \end{aligned} \tag{II. 2}$$

where $v(\frac{-l}{2})$ and $v(\frac{l}{2})$ are the velocity components at the surface of piezoelectric material.

The relation between T and v within the material of the transducer is

$$\frac{dT}{dz} = jwp_{m0}v, \tag{II. 3}$$

and

$$\frac{dv}{dz} = jwS. \tag{II. 4}$$

The total current through the transducer is

$$I_3 = jwAD\,. \qquad \text{(II. 5)}$$

The voltage across the transducer is:

$$V_3 = \int_{-l/2}^{l/2} E dz\,. \qquad \text{(II. 6)}$$

The current is conserved within the structure; therefore D must be uniform with z. Using the following equations:

$$\begin{aligned} D &= \varepsilon^s E + eS, \\ T &= c^E S - eE, \end{aligned} \qquad \text{(II. 7)}$$

we simplify T by eliminating E,

$$T = c^D S - hD\,, \qquad \text{(II. 8)}$$

where h is known as *transmitting constant*, defined as:

$$h = \frac{e}{\varepsilon^S}\,, \qquad \text{(II. 9)}$$

with

$$c^D = c^E\left(1 + \frac{e^2}{c^E \varepsilon^S}\right) = c^E(1 + K^2)\,, \qquad \text{(II. 10)}$$

If we eliminate T and S from Eqs. (II.3), (II.5) and (II.8), then v obeys the wave equation:

$$\frac{d^2 v}{dz^2} + \frac{w^2 p_{m0}}{c^D} v = 0\,, \qquad \text{(II. 11)}$$

which has the solutions

$$v = v_F e^{-j\bar{\beta}_a z} + v_B e^{j\bar{\beta}_a z}\,, \qquad \text{(II. 12)}$$

and

$$T = T_F e^{-j\bar{\beta}_a z} + T_B e^{j\bar{\beta}_a z} - hD\,. \qquad \text{(II. 13)}$$

The subscripts F and B stand for forward and backward propagating waves, respectively, where:

$$\bar{\beta}_a = w(\frac{p_{m0}}{c^D})^{1/2}, \qquad \text{(II. 14)}$$

is the propagation constant and

$$\bar{Z}_0 = (p_{m0}c^D)^{1/2}, \qquad \text{(II. 15)}$$

is the acoustic impedance besides,

$$T_F = -\bar{Z}_0 v_F, \qquad \text{(II. 16)}$$

$$T_B = \bar{Z}_0 v_B\,. \qquad \text{(II. 17)}$$

Using the boundary conditions of Eq (II.2) and Eq. (II.12), we see that:

$$v = \frac{-v_2 \sin[\bar{\beta}_a(z + l/2)] + v_1 \sin[\bar{\beta}_a(l/2 - z)]}{\sin(\bar{\beta}_a l)}\,. \qquad \text{(II. 18)}$$

Substituting the results in Eq. (II.2) and (II.4)-(II.7), it follows after some algebra that

$$\begin{bmatrix} F_1 \\ F_2 \\ V_3 \end{bmatrix} = -j \begin{bmatrix} Z_C \cot\bar{\beta}_a l & Z_C \operatorname{cosec}\bar{\beta}_a l & \frac{h}{w} \\ Z_C \operatorname{cosec}\bar{\beta}_a l & Z_C \cot\bar{\beta}_a l & \frac{h}{w} \\ \frac{h}{w} & \frac{h}{w} & \frac{1}{wC_0} \end{bmatrix} \begin{bmatrix} v_1 \\ v_2 \\ I_3 \end{bmatrix} \qquad \text{(II. 19)}$$

APPENDIX III

Derivation of F_1 / V_s

The electrical ports of the proposed transducer structure in transmitting mode are connected parallel to each other. In Figure III. 1, electrical ports are connected to V_s.

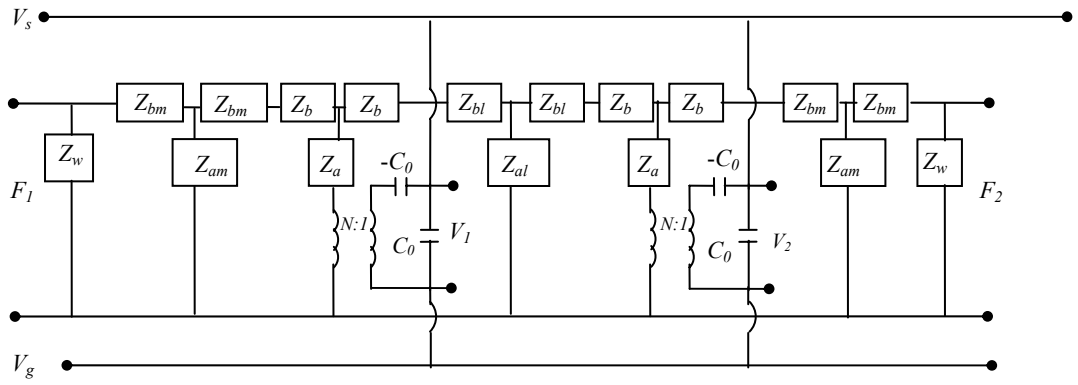

Figure III. 1

We redraw the circuit as depicted in Figure III. 2:

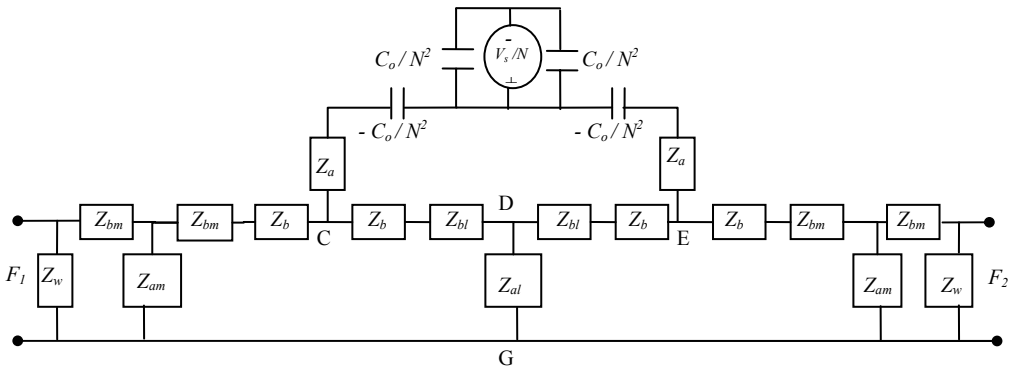

Figure III. 2

We use abbreviations for impedances in between the points, C-D-E-G, where:

$$
\begin{aligned}
Z_{CD} &= Z_b + Z_{bl}, \\
Z_{ED} &= Z_b + Z_{bl}, \\
Z_{DG} &= Z_{al}.
\end{aligned}
\qquad \text{(III. 1)}
$$

We use star – delta transformation at C-D-E-G points. The equivalent impedances are:

$$
\begin{aligned}
Z_{CG} &= \frac{Z_{CD} \times Z_{GD} + Z_{CD} \times Z_{ED} + Z_{ED} \times Z_{GD}}{Z_{ED}}, \\
Z_{CE} &= \frac{Z_{CD} \times Z_{GD} + Z_{CD} \times Z_{ED} + Z_{ED} \times Z_{GD}}{Z_{GD}}, \\
Z_{EG} &= \frac{Z_{CD} \times Z_{GD} + Z_{CD} \times Z_{ED} + Z_{ED} \times Z_{GD}}{Z_{CD}}.
\end{aligned}
\qquad \text{(III. 2)}
$$

Figure III. 2 is redrawn as shown in Figure III. 3:

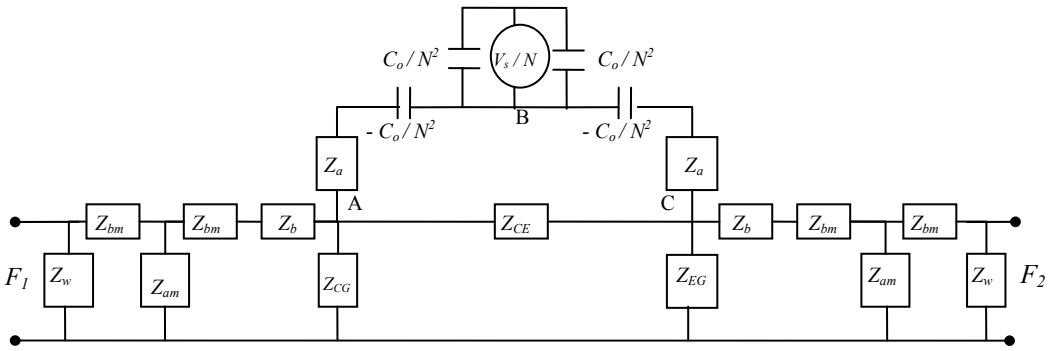

Figure III. 3

We make another simplification so that:

$$
\begin{aligned}
Z_{AB} &= Z_a - \frac{N^2}{jwC_0}, \\
Z_{BC} &= Z_a - \frac{N^2}{jwC_0}, \\
Z_{AC} &= Z_{CE}.
\end{aligned}
\qquad \text{(III. 3)}
$$

We use the delta - star transformation at the A-B-C junction points (Figure III. 4). The equivalent impedances are:

$$Z_{AN} = \frac{Z_{AC} \times Z_{AB}}{Z_{AC} + Z_{AB} + Z_{BC}},$$
$$Z_{BN} = \frac{Z_{AB} \times Z_{BC}}{Z_{AC} + Z_{AB} + Z_{BC}}, \qquad \text{(III. 4)}$$
$$Z_{CN} = \frac{Z_{AC} \times Z_{BC}}{Z_{AC} + Z_{AB} + Z_{BC}}.$$

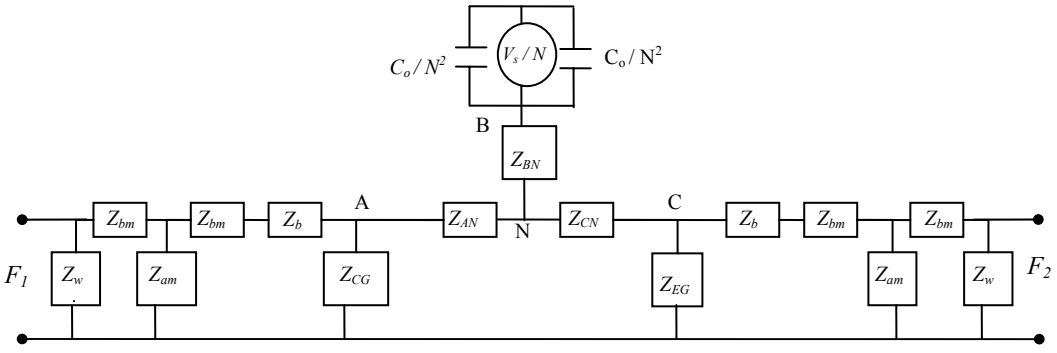

Figure III. 4

We rearrange the circuit as shown in Figure III. 5:

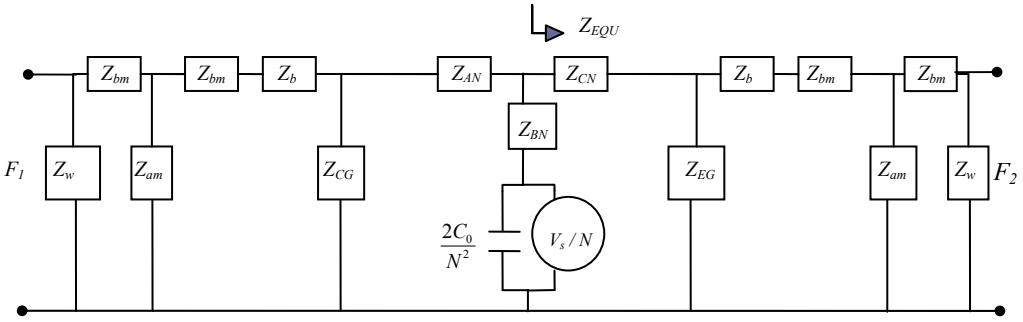

Figure III. 5

Rearranging the circuit is simplified as below:

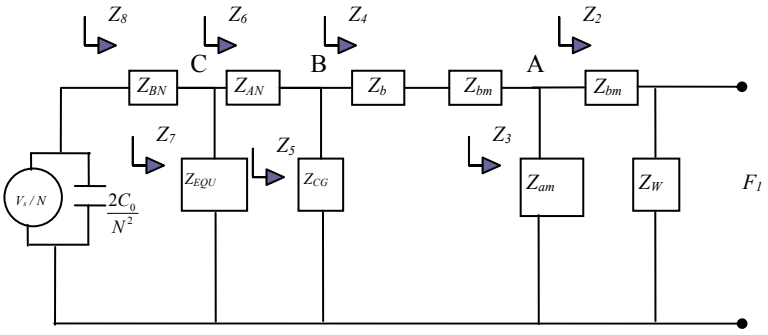

Figure III. 6

We derive the transfer function $\frac{F_1}{V_S}$ using the above circuit diagram, where:

$$Z_1 = Z_W,$$
$$Z_2 = Z_W + Z_{bm},$$

$$\frac{F_1}{F_A} = \frac{Z_1}{Z_2}. \qquad \text{(III. 5)}$$

$$Z_3 = Z_{am} // Z_2,$$
$$Z_4 = Z_b + Z_{bm} + Z_3,$$

$$\frac{F_A}{F_B} = \frac{Z_3}{Z_4}. \qquad \text{(III. 6)}$$

$$Z_5 = Z_{CG} // Z_4,$$
$$Z_6 = Z_{AN} + Z_5,$$

$$\frac{F_B}{F_C} = \frac{Z_5}{Z_6}. \qquad \text{(III. 7)}$$

$$Z_7 = Z_{EQU} // Z_6,$$
$$Z_8 = Z_{BN} + Z_7,$$

$$\frac{F_C}{V_S} = \frac{Z_7}{Z_8} N. \qquad \text{(III. 8)}$$

The transfer function $\frac{F_1}{V_S}$ is:

$$\frac{F_1}{V_S} = \frac{F_1}{F_A}\frac{F_A}{F_B}\frac{F_B}{F_C}\frac{F_C}{V_S}. \qquad \text{(III. 9)}$$

APPENDIX IV

The electrical ports of the transducer structure in receiving mode are connected to feedback amplifiers. Figure IV. 1 shows the circuit diagram of the transducer in receiving mode.

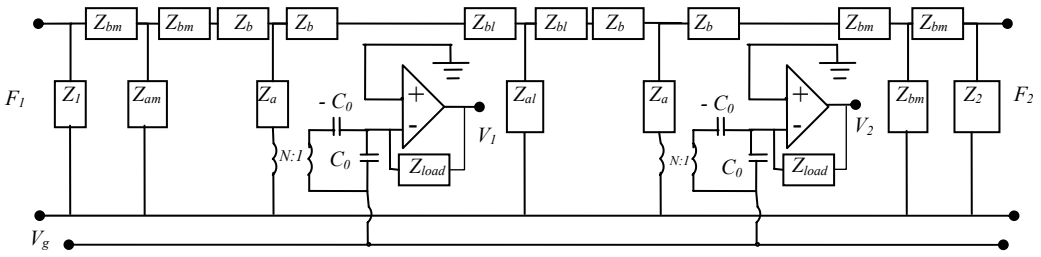

Figure IV. 1

Derivation of V_1 / F_1, when $F_2 = 0$

Figure IV. 2 is the electrical circuit of the receiving transducer, immersed in water and F_2 is short circuited.

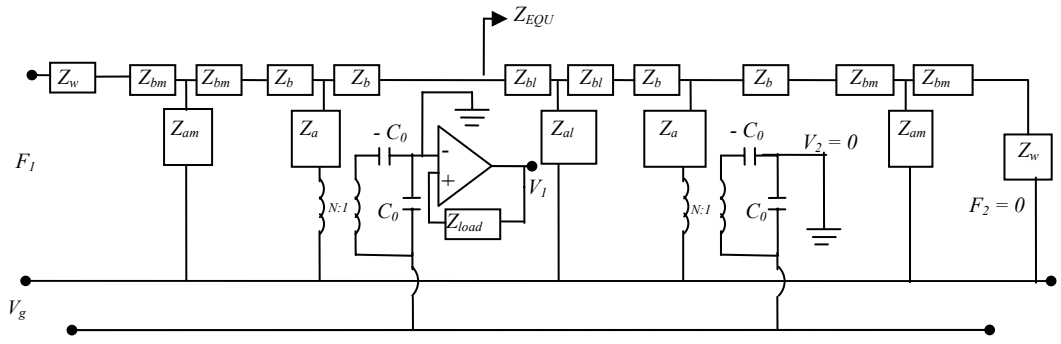

Figure IV. 2

We simplify the impedance seen at right side of the arrow in the above figure as Z_{EQU}, where:

$$Z_1 = Z_W + Z_{bm},$$

$$Z_2 = Z_{am} // Z_w,$$

$$Z_3 = Z_b + Z_{bm} + Z_2,$$

$$Z_4 = (Z_a - \frac{N^2}{jwC_0}) // Z_3, \qquad \text{(IV. 1)}$$

$$Z_5 = Z_b + Z_{bl} + Z_4,$$

$$Z_6 = Z_{al} // Z_5,$$

and

$$Z_{EQU} = Z_{bl} + Z_6. \qquad \text{(IV. 2)}$$

After simplification the circuit looks like the below diagram:

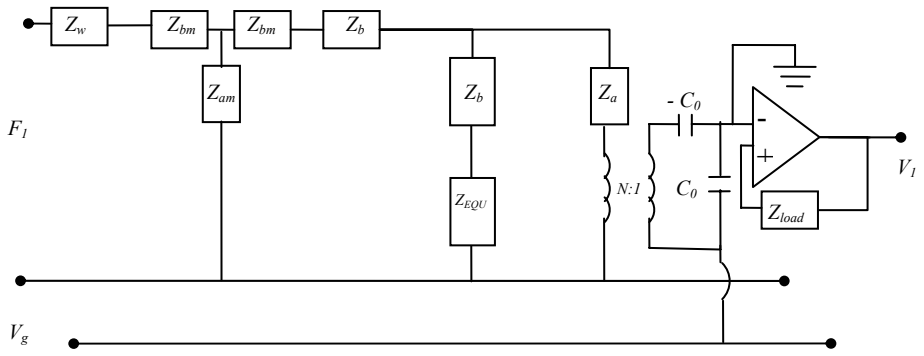

Figure IV. 3

Using Thevenin's theorem, we define F_T and Thevenin impedance, Z_T as shown in Figure IV. 4.

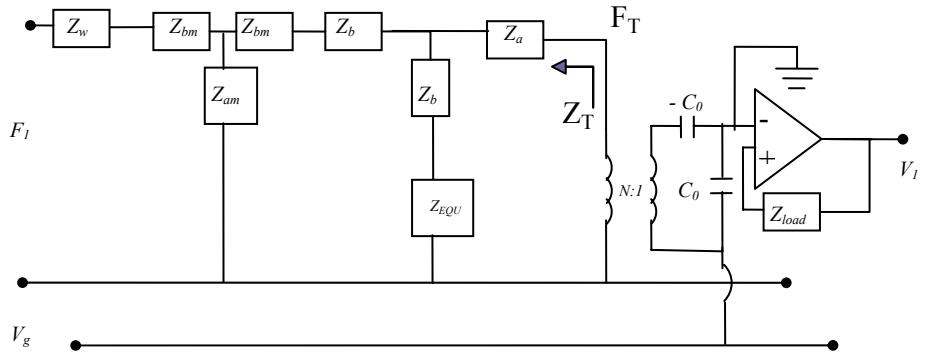

Figure IV. 4

$$\begin{aligned} Z_1 &= Z_W + Z_{bm}, \\ Z_2 &= Z_{am} // Z_1, \\ Z_3 &= Z_b + Z_{bm} + Z_2, \\ Z_4 &= (Z_b + Z_{EQU}) // Z_3, \end{aligned} \qquad \text{(IV. 3)}$$

and

$$Z_T = Z_a + Z_4 . \qquad \text{(IV. 4)}$$

We derive the transfer function $\frac{F_T}{V_1}$ using

Figure IV. **4**

$$\begin{aligned} Z_1 &= Z_b + Z_{EQU}, \\ Z_2 &= Z_{bm} + Z_b + Z_1, \end{aligned} \qquad \text{(IV. 5)}$$

$$\frac{F_T}{F_A} = \frac{Z_1}{Z_2}, \qquad \text{(IV. 6)}$$

$$\begin{aligned} Z_3 &= Z_{am} // Z_2, \\ Z_4 &= Z_w + Z_{bm} + Z_3, \end{aligned}$$

$$\frac{F_A}{F_1} = \frac{Z_3}{Z_4} \quad , \qquad \text{(IV. 7)}$$

$$\frac{F_T}{F_1} = \frac{F_T}{F_A}\frac{F_A}{F_1}, \tag{IV. 8}$$

and

$$F_T = \frac{F_T}{F_A}\frac{F_A}{F_1}F_1 \ . \tag{IV. 9}$$

The circuit looks like below:

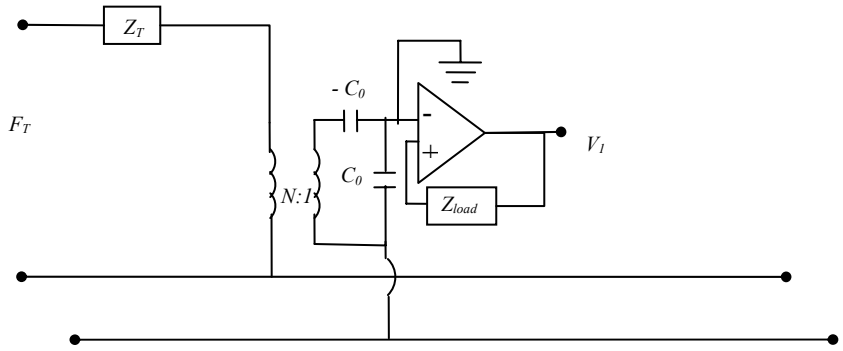

Figure IV. 5

The transfer function is:

$$\frac{V_1}{F_T} = \frac{1}{n}\frac{(N^2 Z_{load})}{(Z_T + N^2 Z_{load} - N^2/(j\omega C_0))}, \tag{IV. 10}$$

$$V_1 = \frac{1}{n}\frac{(N^2 Z_{load})}{(Z_T + N^2 Z_{load} - N^2/(j\omega C_0))}F_T \ . \tag{IV. 11}$$

Derivation of V_2 / F_1 when $F_2 = 0$

In this section, we derive the transfer function V_2 / F_1 when F_2 is short circuited (Figure IV. 6).

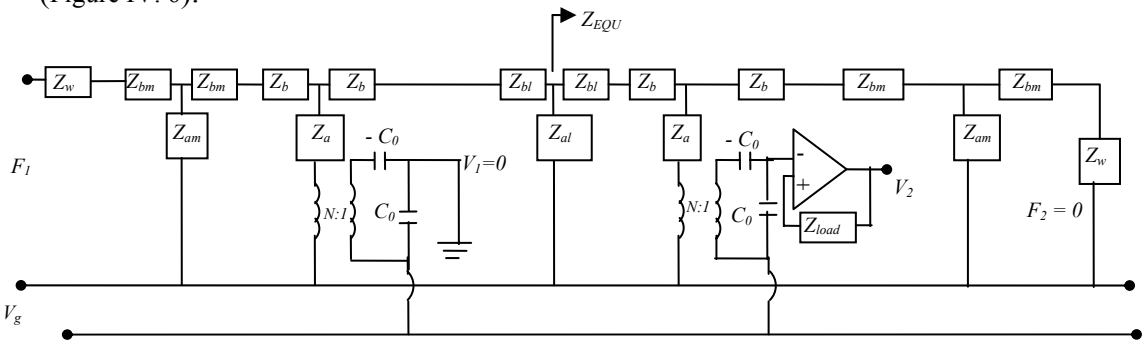

Figure IV. 6

We simplify the impedance seen at the right side of the arrow in the above figure as Z_{EQU}, where:

$$Z_1 = Z_W + Z_{bm},$$
$$Z_2 = Z_{am} // Z_1,$$
$$Z_{EQU} = Z_{bm} + Z_2. \qquad \text{(IV. 12)}$$

The circuit looks like as depicted in Figure IV. 7:

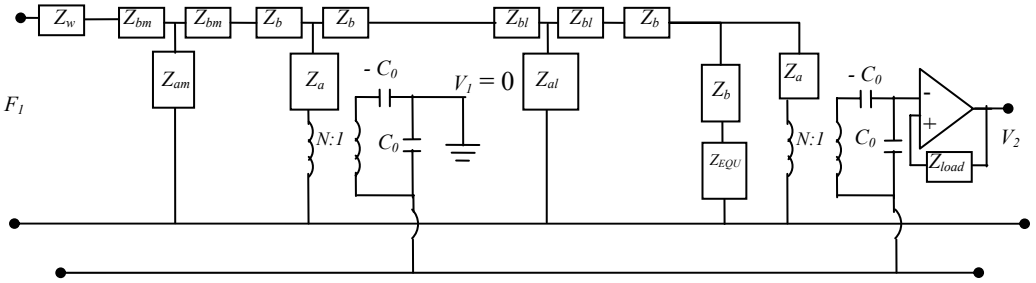

Figure IV. 7

Using Thevenin's theorem, we define Thevenin force, F_T and Thevenin impedance, Z_T:

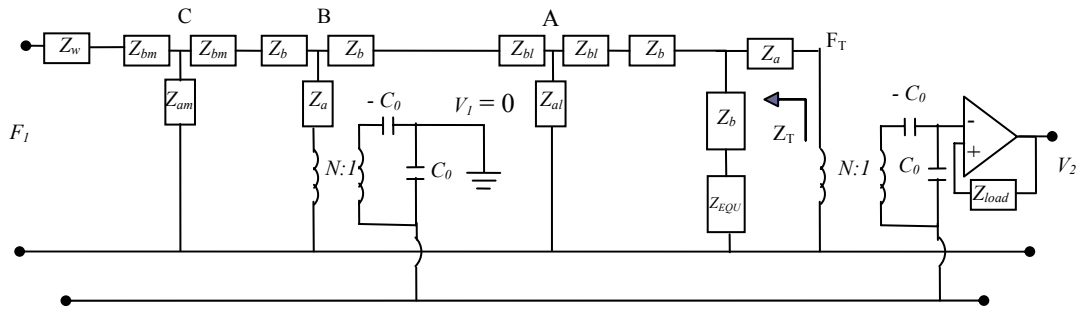

Figure IV. 8

where:

$$Z_1 = Z_W + Z_{bm},$$

$$Z_2 = Z_{am} // Z_1,$$

$$Z_3 = Z_b + Z_{bm} + Z_2,$$

$$Z_4 = (Z_a - \frac{N^2}{jwC_0}) // Z_3,$$

$$Z_5 = Z_b + Z_{bl} + Z_4,$$

$$Z_6 = Z_{al} // Z_5,$$

$$Z_7 = Z_b + Z_{bl} + Z_6,$$

$$Z_8 = (Z_b + Z_{EQU}) // Z_7,$$

and

$$Z_T = Z_a + Z_8. \qquad \text{(IV. 13)}$$

We derive the transfer function $\frac{F_T}{V_1}$ using Figure IV. 8:

$$Z_1 = Z_b + Z_{EQU},$$
$$Z_2 = Z_b + Z_{bl} + Z_1,$$

$$\frac{F_T}{F_A} = \frac{Z_1}{Z_2}. \qquad \text{(IV. 14)}$$

$$Z_3 = Z_{al} // Z_2,$$
$$Z_4 = Z_b + Z_{bl} + Z_3,$$

$$\frac{F_A}{F_B} = \frac{Z_3}{Z_4}. \qquad \text{(IV. 15)}$$

$$Z_5 = (Z_a - \frac{N^2}{jwC_0}) // Z_4,$$
$$Z_6 = Z_b + Z_{bm} + Z_5,$$

$$\frac{F_B}{F_C} = \frac{Z_5}{Z_6}. \qquad \text{(IV. 16)}$$

$$Z_7 = Z_{am} // Z_6,$$
$$Z_8 = Z_w + Z_{bm} + Z_7,$$

$$\frac{F_C}{F_1} = \frac{Z_7}{Z_8}. \qquad \text{(IV. 17)}$$

As a result:

$$\frac{F_T}{F_1} = \frac{F_T}{F_A}\frac{F_A}{F_B}\frac{F_B}{F_C}\frac{F_C}{F_1}, \qquad \text{(IV. 18)}$$

and

$$F_T = \frac{F_T}{F_A}\frac{F_A}{F_B}\frac{F_B}{F_C}\frac{F_C}{F_1}F_1. \qquad \text{(IV. 19)}$$

After rearranging Figure IV. 8 the circuit becomes as shown in Figure IV. 9.

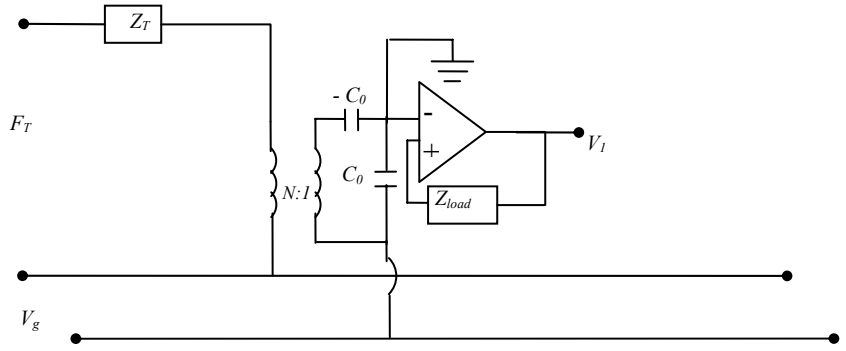

Figure IV. 9

where

$$\frac{V_1}{F_T} = \frac{1}{n}\frac{(N^2 Z_{load})}{(Z_T + N^2 Z_{load} - N^2/(j\omega C_0))}, \qquad \text{(IV. 20)}$$

$$V_1 = \frac{1}{n}\frac{(N^2 Z_{load})}{(Z_T + N^2 Z_{load} - N^2/(j\omega C_0))}F_T. \qquad \text{(IV. 21)}$$

APPENDIX V

Derivation of Propagation Function

The propagation functions derived in this section are due to radiated acoustic waves from the acoustic port of a transducer which are sensed at the acoustic port of another transducer. The transmitting acoustic face and receiver are placed at the same half – space as described in Chapter 5.

The potential at any point ($z \geq 0$) is derived to be in the form:

$$\phi = -\frac{1}{2\pi}\int_{S_1} u_z(x,y,z)\frac{e^{-jkR_1}}{R_1}ds_1 \,. \qquad \text{(V. 1)}$$

where R_1 is the distance between the source point (x,y,z) and the point where potential due to acoustic waves is calculated $(x',y',-z_0)$. We assume that $x' \ll x$ and $y' \ll y$. We simplify R_1 as R:

$$R_1 = \sqrt{(x-x')^2 + (y-y')^2 + (z-z_0)^2}, \qquad \text{(V. 2)}$$

where

$$\begin{aligned} R_1 &= \sqrt{(x^2 - 2xx' + x'^2) + (y^2 - 2yy' + y'^2) + (z^2 - 2zz_0 + {z_0}^2)}, \\ R &= \sqrt{x^2 + y^2 + z^2}. \end{aligned} \qquad \text{(V. 3)}$$

R is the distance between the center of the source and (x', y', z_0) receiving point (x, y, z) as shown in Figure V. 1. We simplify denominator and numerator radius values of Eq. (V.1) as follows:

$$\begin{aligned} &\text{(Numerator)} \qquad R_1 = R(1 - \frac{x'x}{R^2} - \frac{y'y}{R^2} - \frac{z_0 z}{R^2}), \\ &\text{(Denominator)} \qquad R_1 = R. \end{aligned} \tag{V. 4}$$

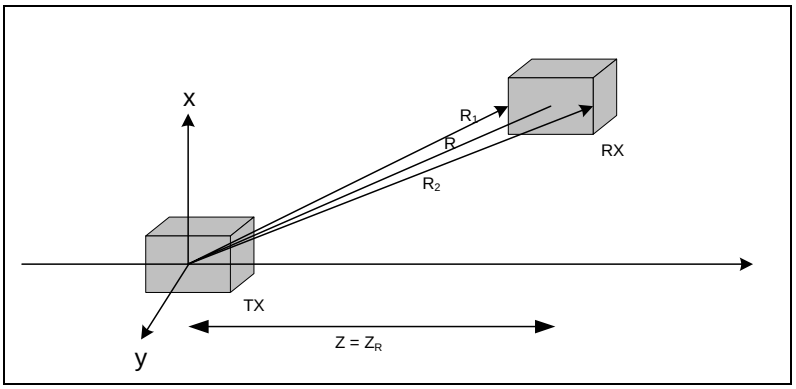

Figure V. 1. Alignment of source and receiver

After substituting Eq. (V- 4) into Eq. (V – 1), the potential becomes:

$$\phi = -\frac{u_0}{2\pi} \int_{S_1} \frac{e^{-jkR} e^{\frac{jk(x'x+y'y)}{R}}}{R} e^{\frac{jkz_0 z}{R}} dx'dy' . \tag{V. 5}$$

Integrating over the front acoustical port of the receiver S_1 where $-x_0 \le x' \le x_0$ and $-y_0 \le y' \le y_0$:

$$\phi = -\frac{u_0}{2\pi} \frac{e^{-jkR}}{R} e^{\frac{jkz_0 z}{R}} \int_{-x_0}^{x_0} e^{\frac{jkx'x}{R}} dx' \int_{-y_0}^{y_0} e^{\frac{jky'y}{R}} dy' , \tag{V. 6}$$

results with the below definition:

$$\phi = -\frac{u_0}{2\pi}(2x_0 2y_0)\frac{e^{-jkR}}{R}e^{\frac{jkz_0 z}{R}}\frac{\sin(\frac{kx_0 x}{R})}{(\frac{kx_0 x}{R})}\frac{\sin(\frac{ky_0 y}{R})}{(\frac{ky_0 y}{R})}. \qquad \text{(V. 7)}$$

Using the equation $\frac{\sin a}{a} = \operatorname{sinc} a$, the potential is simplified to:

$$\phi = -\frac{u_0}{2\pi}(2x_0 2y_0)\frac{e^{-jkR}}{R}e^{\frac{jkz_0 z}{R}}\sin c(\frac{kx_0 x}{R})\sin c(\frac{ky_0 y}{R}). \qquad \text{(V. 8)}$$

We integrate the total density over the front acoustic face to calculate the net force above it:

$$F(z - z_0) = \int_{-x_0}^{x_0}\int_{-y_0}^{y_0} p\,dxdy. \qquad \text{(V. 9)}$$

We use the expression:

$$p = w^2\rho\phi, \qquad \text{(V. 10)}$$

and substitute Eq. (V – 8) and Eq. (V – 10) into Eq. (V – 9). The force on the front acoustic face becomes:

$$F(z - z_0) = -\int_{-x_0}^{x_0}\int_{-y_0}^{y_0} w^2\rho\frac{u_0}{2\pi}(2x_0 2y_0)\frac{e^{-jkR}}{R}e^{\frac{jkz_0 z}{R}}\sin c(\frac{kx_0 x}{R})\sin c(\frac{ky_0 y}{R})dxdy \qquad \text{(V. 11)}$$

We calculate the force formed on the front acoustic port when the receiver is rotated (θ, φ) degrees with respect to the transmitter (Figure V. 2). We model this case such that we keep the receiver aligned at the $z = z_R$ plane and rotate the

transmitter around the receiver to distribute the affect of rotation to the transmitter (Figure V. 3). It is seen that a point on the transmitting acoustic port (*x,y,z)* shifts to the point $(-z_R \sin\theta, z_R \sin\varphi\cos\theta, z_R(1-\cos\varphi\cos\theta))$. The distance between the centers of the transducers then becomes:

$$R = [(x + z_R \sin\theta)^2 + (y - z_R \sin\varphi\cos\theta)^2 + (z - z_R + z_R \cos\varphi\cos\theta))]^{1/2},$$

$$\begin{aligned} R = [&x^2 + z_R{}^2 \sin^2\theta + 2xz_R \sin\theta + y^2 + z_R{}^2 \sin^2\varphi\cos^2\theta - 2yz_R \sin\varphi\cos\theta \\ &+ z^2 + z_R{}^2 + z_R{}^2 \cos^2\theta\cos^2\varphi - 2zz_R + 2zz_R \cos\varphi\cos\theta - 2z_R{}^2 \cos^2\varphi\cos^2\theta]^{1/2}. \end{aligned} \quad \text{(V. 12)}$$

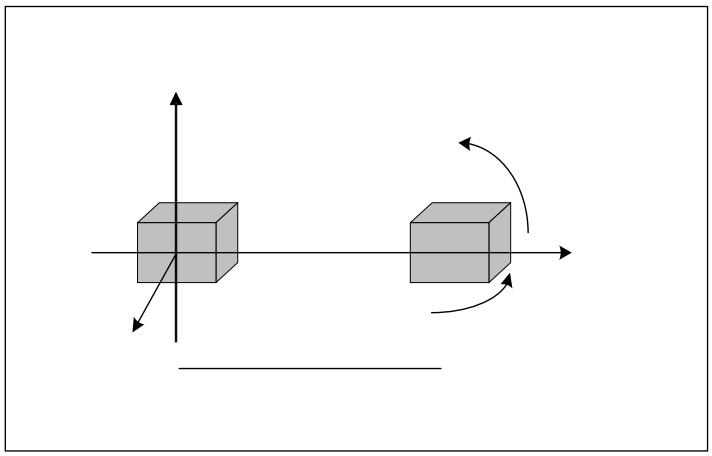

Figure V. 2. Rotating the receiver (θ, φ) degrees.

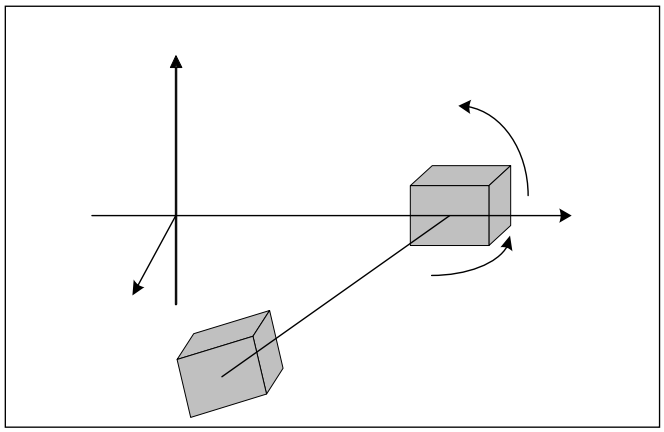

Figure V. 3. Moving and rotating the transmitter around the receiving transducer.

The distance between the source and the receiver, R when z = $z_R - z_0$ and $z_0 \ll z_R$ becomes:

$$R=[x^2+y^2+{z_R}^2+{z_0}^2+2xz_R\sin\theta-2yz_R\sin\varphi\cos\theta-2z_Rz_0\cos\varphi\cos\theta]^{1/2}, \qquad \text{(V. 13)}$$

$$x^2+y^2+{z_R}^2={z_R}^2,$$

$$R=z_R(1-\frac{z_0}{z_R}\cos\varphi\cos\theta+\frac{x}{z_R}\sin\theta-\frac{y}{z_R}\cos\theta) \qquad \text{(V. 14)}$$

Substituting Eq. (V – 14) into Eq. (V – 11) and taking the derivative of force, *F* becomes:

$$F(z-z_0)=-w^2\rho\frac{u_0}{2\pi}(2x_02y_0)\frac{e^{-jkZ_R}}{Z_R}e^{\frac{jkz_0z}{R}}\sin c(\frac{kx_0x}{R})\sin c(\frac{ky_0y}{R})e^{\frac{jkz_0z}{R}}e^{jkz_0\cos\theta\cos\varphi} \qquad \text{(V. 15)}$$
$$(2x_02y_0)\sin c(kx_0\sin\theta)\sin c(ky_0\sin\varphi\cos\theta)$$

Since, the particle displacement u_0 is:

$$u_0=\frac{\dot{u}_0}{jw}=\frac{F_0}{jwZ_0}, \qquad \text{(V. 16)}$$

and the characteristic impedance Z_0 equals:

$$Z_0=A\rho c, \qquad \text{(V. 17)}$$

we can simplify the first three terms of Eq. (V.15) as follows:

$$\rho w^2u_0=\rho w^2\frac{F_0}{jwZ_0}=\rho w^2\frac{F_0}{jwA\rho c}=\frac{kF_0}{jA}=\frac{kF_0}{j(2x_02y_0)}. \qquad \text{(V. 18)}$$

Then, the total force at the front acoustic port of the receiving transducer becomes:

$$F(z-z_0)=-\frac{kF_0}{j2\pi}A\frac{e^{-jkR}}{R}\sin c(\frac{kx_0x}{R})\sin c(\frac{ky_0y}{R})e^{\frac{jkz_0z}{R}}e^{jkz_0\cos\theta\cos\varphi} \qquad \text{(V. 19)}$$
$$\sin c(kx_0\sin\theta)\sin c(ky_0\sin\varphi\cos\theta).$$

In a similar way the electrical force sensed at the rear acoustic port, $F(z+z_0)$, of the receiving transducer can be found as:

$$F(z+z_0) = -\frac{kF_0}{j2\pi} A \frac{e^{-jkR}}{R} \sin c(\frac{kx_0 x}{R}) \sin c(\frac{ky_0 y}{R}) e^{\frac{jkz_0 z}{R}} e^{-jkz_0 \cos\theta \cos\varphi} \sin c(kx_0 \sin\theta) \sin c(ky_0 \sin\varphi \cos\theta). \quad \text{(V. 20)}$$